PROPAGATION OF MULTIWAVELENGTH LASER RADIATION THROUGH ATMOSPHERIC TURBULENCE

J. Richard Kerr

Oregon Graduate Center for Study and Research

Prepared for:

Rome Air Development Center
Advanced Research Projects Agency

15 January 1973

RADC-TR-73-54
Technical Report
January 1973

PROPAGATION OF MULTIWAVELENGTH LASER RADIATION THROUGH ATMOSPHERIC TURBULENCE

Oregon Graduate Center for
Study and Research

Sponsored by
Defense Advanced Research Projects Agency
ARPA Order No. 1279
Amend. 5

Rome Air Development Center
Air Force Systems Command
Griffiss Air Force Base, New York

Security Classification

DOCUMENT CONTROL DATA - R & D

Security classification of title, body of abstract and indexing annotation must be entered when the overall report is classified

1. ORIGINATING ACTIVITY (Corporate author)
Oregon Graduate Center for Study and Research
Beaverton, Oregon 97005

2a. REPORT SECURITY CLASSIFICATION
Unclassified

2b. GROUP

3 REPORT TITLE
Propagation of Multiwavelength Laser Radiation through Atmospheric Turbulence

4. DESCRIPTIVE NOTES (Type of report and, inclusive dates)
Quarterly report, September 15, 1972 - December 15, 1972

5. AUTHOR(S) (First name, middle initial, last name)
J. Richard Kerr

6. REPORT DATE	7a. TOTAL NO. OF PAGES	7b. NO. OF REFS
January 15, 1973	74 81	48

8a. CONTRACT OR GRANT NO.	9a. ORIGINATOR'S REPORT NUMBER(S)
F30602-72-C-0470	1174-2
b. PROJECT NO. 1279	
c. Program Code Number 3E20	9b. OTHER REPORT NO(S) (Any other numbers that may be assigned this report)
d. Arpa Order Number 1279 Amend. 5	RADC-TR-73-54

10. DISTRIBUTION STATEMENT
Approved for public release, distribution unlimited.

11. SUPPLEMENTARY NOTES	12. SPONSORING MILITARY ACTIVITY
Monitored by: Raymond P. Urtz, Jr. RADC (OCSE), GAFB, N.Y. 13440	Advanced Research Projects Agency Washington, D.C. 20301

13. ABSTRACT

This report summarizes progress on three currently active efforts in the investigation of laser beam scintillations due to atmospheric turbulence. These topics are (1) multiwavelength scintillation over a long horizontal path with a very high integrated-path turbulence level; (2) finite-beam or transmitter aperture effects including beam wander, spread, and scintillation; and (3) turbulence intermittency effects.

The long path results are presented in detail. Saturation of scintillations was observed at 10.6 μm, with the evolution of very small and very large scintillation scale sizes, as predicted in recent theoretical work. The effects of atmospherically-induced beam wander and spread on mean target illumination are explored theoretically, as are the fading effects of wander and finite-beam scintillations. Certain inconsistencies in the literature pertaining to these effects are resolved, and the advantages to be expected from an ongoing beam-wander-cancellation experiment are described. The effects of turbulence intermittencies are analyzed in terms of a discrete slab model, including the possible influence of the inner scale. The intermittency problem is restated and experimental plans are described.

DD FORM 1 NOV 65 1473 (PAGE 1)
S/N 0101-807-6811

19

UNCLASSIFIED
Security Classification

A-31408

14 KEY WORDS	LINK A		LINK B		LINK C	
	ROLE	WT	ROLE	WT	ROLE	WT
Propagation						
Turbulence						
Atmospheric Optics						
Scintillation						
10.6 Microns						

PROPAGATION OF MULTIWAVELENGTH LASER RADIATION THROUGH ATMOSPHERIC TURBULENCE

J. Richard Kerr

Contractor: Oregon Graduate Center for Study and Research
Contract Number: F30602-72-C-0470
Effective Date of Contract: 15 June 1972
Contract Expiration Date: 15 June 1973
Amount of Contract: $65,775.00
Program Code Number: 3E20

Principal Investigator: Dr. J. Richard Kerr
Phone: 503 645-1121

Project Engineer: Mr. Raymond P. Urtz, Jr.
Phone: 315 330-3145

This research was supported by the Defense Advanced Research Projects Agency of the Department of Defense and was monitored by Raymond P. Urtz, Jr., RADC (OCSE), GAFB, NY 13441, under Cont F30603-72-C-0470.

Summary

This report summarizes progress on three currently active efforts in the investigation of laser beam scintillations due to atmospheric turbulence. These topics are (1) multiwavelength scintillation over a long horizontal path with a very-high integrated-path turbulence level; (2) finite-beam or transmitter-aperture effects including beam wander, spread, and scintillation; and (3) turbulence intermittency effects.

The long path results are presented in detail. Saturation of scintillations was observed at 10.6 μm, and the behavior far into saturation was explored at 4880 Å. The evolution of very small and very large scintillation scale sizes was observed, as predicted in a recent theoretical treatment. The effects of atmospherically-induced beam wander and spread on mean target-illumination are explored theoretically, as are the fading effects owing to combined wander and scintillations. Certain inconsistencies in the literature pertaining to these effects are resolved, and the advantages to be expected from an ongoing beam-wander-cancellation experiment are described. Turbulence intermittence is modelled in terms of discrete slabs of turbulence, and inner scale effects are analyzed. The intermittency problem is redefined and experimental plans are described.

TABLE OF CONTENTS

I. Introduction

During the reporting period, work was conducted on long-path scintillations, finite-beam effects, and turbulence intermittency effects.

The long-path experiments have been completed, the data analyzed, and the results interpreted. This effort is described in detail in Section II. Very interesting new results were obtained regarding saturation at 10 μm wavelengths, the evolution of new scintillation scale lengths at large integrated-path turbulence levels, and the behavior far into saturation.

In Section III, the theoretical predictions of finite-beam effects are reviewed in detail, including beam wander, instantaneous spread, and scintillation. Apparent inconsistencies and contradictions in various treatments in the literature are resolved, and the results are applied to the specification of important new experiments in this area. These include the cancellation of beam wander through the use of a reciprocal property of turbulence propagation.

In Section IV, we redefine the turbulence intermittency problem with regard to propagation effects, and present some pertinent analytical results.

II. Long-Path Scintillations

The purpose of these experiments was to measure the properties of scintillations over the longest, lowest path which can be reasonably achieved, in order to encounter the highest integrated-path turbulence level possible. The experiments were conducted with simultaneous, coincident virtual-point-sources at visible and middle-infrared wavelengths. The measurements are itemized in Table I, and include turbulence strength, meteorological parameters, and scintillation statistics. The turbulence and scintillation quantities are defined in Ref. 1, and the general instrumentation and field facilities are described in Refs. 2 and 3, respectively.

The experimental parameters are summarized in Table II. Due to the fact that the experiments took place over such a long, uniform path near the ground, long-term vertical beam-bending due to thermal gradients was significant. This was manifested as a mirage effect during early morning hours, and conversely as a looming horizon during afternoon or high-turbulence hours. As a result of the latter, it was necessary to utilize elevated transmitters and receivers to maintain an unobstructed path during peak turbulence periods. Significant difficulties were experienced with laser reliability, such that reliable data were not taken until the final few high-turbulence days of summer. However, the quantity of data is considered sufficient for the conclusions drawn below.

Major objectives of these experiments were the measurement of saturation[1] of log amplitude variance and related effects at the 10.6 μm wavelength, the investigation of scintillation statistics at a visible wavelength far into the saturation region, and the examination of large-integrated-path turbulence effects on scintillation correlation scales and hence receiver aperture-smoothing. In the following sections, we discuss log amplitude variance, covariance, scintillation spectra, probability distributions, and receiver aperture smoothing respectively.

TABLE I. Experimental Measurements.

Strength of turbulence (C_n^2) from microthermal probes

Vertical temperature gradient

Wind velocity

Log amplitude variance

Log amplitude covariance

Log amplitude probability distribution

Scintillation spectrum

Receiver aperture smoothing

TABLE II. Experimental Parameters.

Path length: 6.0 km

Path description: Farmland, flat to within $\pm$ 0.5 m

Transmitter height: 6.1 m

Receiver height: 3.5 m

Wavelengths (simultaneous, coincident): 4880 Å, 10.6 μm

Transmitter beam configuration: Virtual point sources (Fresnel number $<10^{-3}$)

Receiver aperture: 6 mm

Receiver dynamic range: >80 dB

Receiver averaging time: 60 sec

Aperture-smoothing receiver: 0.6-32 cm

Resolution of spectral measurements: 1 Hz

Receiver bandwidth: 1 kHz

Microthermal probe separation for C_n^2: 10 cm

Microthermal probe height: 1.8 m

Microthermal averaging time: 300 sec

A. Log Amplitude Variance

Experimental log amplitude variances (σ_E^2) were obtained from probability distributions. A typical diurnal behavior for a cloudless day is shown in Figure 1. The unusually high values of σ_E^2 for 4880 Å in the early morning were due to poorly developed turbulence structure,[2] and there is evidence that the presence of light ground fog during that period further increased these anomalous fluctuations. The data show that for this very long, low path configuration the variance at 4880 Å was nearly always saturated. As discussed below, the lower extreme of these variances is not indicative of an asymptote for high turbulence. Outside of the anomalous-turbulence period, the 10.6 μm variances were seen to saturate in mid-morning.

The variances measured at 10.6 μm are shown in Figure 2 vs. the strength of turbulence taken at a height of 1.8 m. For the first time, saturation is clearly indicated at this wavelength. As discussed below, the abscissa is not highly meaningful without a correction due to variable beam-refraction. The saturation level appears to be somewhat below the 0.6 value typical of shorter wavelengths;[1,2] according to a recent theoretical treatment, this may very likely be due to the effects of the finite outer scale of turbulence.[4]

Similar data are given in Figure 3 for 4880 Å. The logarithmic slope beyond saturation is near the (-1/6) value predicted by deWolf.[5] However, as discussed below and in following sections, corrections are required for beam refraction and covariance scale effects, and the agreement is probably fortuitous.

Since the strength of turbulence depends significantly upon the height above ground, a more meaningful presentation of the data is obtained by correcting for beam refraction and earth curvature. A useful abscissa is then the theoretical variance σ_T^2 as predicted from the Rytov or first-order theory.[1] If we define the path-length variable as (x), we may write[1,6]

$$\sigma_T^2 = 0.56\, k^{7/6} \int_0^L C_n^2(x) \left(\frac{x}{L}\right)^{5/6} (L-x)^{5/6}\, dx \quad , \tag{1}$$

where L is the total pathlength and k is the optical/infrared wavenumber. In accordance with Wyngaard and Izumi,[7] the height dependence of C_n^2 is taken as the minus 4/3 exponent. We may then account for beam refraction and earth curvature by writing

$$\sigma_T^2 = 0.56\, k^{7/6}\, z_o^{4/3}\, C_n^2(z_o)\, L^{-5/6} \int_0^L z(x)^{-4/3}\, x^{5/6}\, (L-x)^{5/6}\, dx, \tag{2}$$

where z is the beam height and z_o is a reference height.

It still remains to determine z(x), which depends upon the vertical gradient in the refractive index, and hence on the temperature gradient. Our measurements of the vertical temperature distribution show that the temperature can be reasonably represented as linear over the range involved. The gradient (B) is small, and the resultant refractive index may also be approximated as being linear with height:

$$\frac{dn(z)}{dz} \sim B \quad . \tag{3}$$

The trajectory of the beam through such a medium is parabolic. With the use of the transmitter and receiver heights as boundary conditions, and the addition of the earth's curvature, the path may be found for each measured value of B. Representative profiles are given in Table III. The lowest beam heights under negative-gradient conditions, which occur during the high turbulence part of the day, were comfortably above ground cover and agreed with visual observations.

TABLE III. Beam Height (in Meters) Vs. Temperature Gradient and Distance.

Thermal Gradient (^{o}K/m)	Distance from Transmitter (km)						
	0	1	2	3	4	5	6
+0.4	6.1	7.3	7.8	7.7	6.9	5.5	3.5
-0.06	6.1	5.0	4.2	3.6	3.3	3.3	3.5
-0.2	6.1	4.5	3.3	2.7	2.5	2.3	2.5

With the insertion of the proper trajectories into Eq. (2), the plots of Figures 4 and 5 are obtained for 10.6 μm and 4880 Å respectively. A linear regression analysis for Figure 5 yields a log-log slope of -0.48, with a correlation coefficient of 0.78, and no apparent asymptote. This does not support a recent theoretical prediction[5] of (-1/6), and there does not appear to be an asymptote.

We question the results of Ref. 5 on the grounds that they strongly involve the inner scale; in particular they predict saturation at vanishingly small turbulence levels for inner scales approaching zero, and this does not seem reasonable. However, as pointed out in the following sections, there is an apparent contribution to the log amplitude variance at 4880 Å which is due to very small scintillation correlation-scales, and both electronic and (6 mm) receiver aperture filtering have reduced this component in the present data. A correction for this effect will decrease the slope magnitude in Figure 5 to an unknown but possibly significant degree.

A plot of the experimental variance at 4880 Å vs. that at 10.6 μm is shown in Figure 6. Similar plots for shorter wavelengths appear in Refs. 2 and 8, and illustrate the failure of the $k^{7/6}$ dependence of Eq. (1) in saturation.

B. Log Amplitude Covariance

The transverse log amplitude correlation length (r_a), which is defined from the 1/e point of the measured covariance curve, is shown as a function of C_n^2 in Figure 7. A significant effect is observed at stronger turbulence levels, where r_a is seen to markedly decrease and increase at 10.6 μm and 4880 Å wavelengths respectively. This agrees with a trend observed in earlier work.[2]

In order to better understand the significance of these results, it is necessary to consider the detailed shape of the covariance curves. Typical curves for 10.6 μm are shown in Figure 8. At low C_n^2, the function approximates the theoretical prediction except for large separations, where outer scale effects may enter. However, as C_n^2 increases, two new and highly disparate scale lengths emerge, such that for strong turbulence, the scintillation patches are quite small with a significant residual correlation over large separations. This unusual manifestation of multiple scattering was predicted in a recent two-dimensional analysis by Brown.[4] It may be noted that the change in vertical beam trajectory, such that the highest turbulence level is encountered near midpath at high overall turbulence strengths, would imply the emergence of a single intermediate scale size and is hence not pertinent here.

This effect is even more pronounced at 4880 Å, as shown in Figure 9. In fact, the effect is so extreme as to suggest that significant spatial and electronic filtering of the small scintillation patches is occurring at high turbulence levels; this is confirmed in the next section, and indicates that e.g. for curve D, a very sharp initial fall-off has been obscured and the normalization is incorrect. This explains the behavior seen in Figure 7. Visually, at high turbulence levels the very large correlation patches are observed, and the very small patches are washed out due to eye response. Note that these results imply very poor receiver-aperture-smoothing, as will be confirmed below.

C. Scintillation Spectra

The scintillation power spectra at 10.6 μm are shown in Figures 10 and 11 for the same turbulence levels as in Figure 8, and corroborate the behavior shown in the latter figure. As the turbulence increases, much more energy appears at high frequencies; a concurrent shift to low frequencies is obscured by the low-frequency cutoff of the spectrum analyzer.

The results at 4880 Å (Figures 12 and 13) apparently fail to encompass sufficient low and high frequency ranges to manifest the extreme scales emerging in Figure 9. An exception is the transitional curve (B). A similar plot extending to 1 kHz is not substantially different, and quantitative spectral results above that frequency were not obtained due to electronic and spatial (6 mm receiver) filtering.

The fact that, at these very large integrated-path turbulence levels, scintillations occur at frequencies above one kilohertz was verified by direct observation of the signal (Figure 14). This interesting behavior confirms that the initial part of curve (D) in Figure 9 has been obscured by instrumental effects. A similar display at 10.6 μm is given in Figure 15. The emerging low frequency components were also readily visible on appropriate time scales.

It is recognized that the spectral results of Figures 10-13 are of only semiquantitative significance since the wind velocity was variable over the time periods spanned. An attempt to normalize out this effect as in Ref. 2 was unsuccessful, due to the complicated nature of the covariance and spectral curves and the corresponding inadequacy of single-parameter descriptions (e.g. r_a).

D. Probability Distributions

Earlier theoretical treatments predicted Rayleigh amplitude statistics at large turbulence strengths.[9] Experimental values (Figure 16) have confirmed that the scintillations remain substantially log normal, with no indication of Rayleigh behavior. This agrees with more recent treatments.[5] It may be noted that, in the Rayleigh case, the "dynamic range" between two probability levels

is an invariant number and that the present data are completely sufficient to rule out a Rayleigh distribution.

E. Receiver Aperture Smoothing

The covariance results of Figures 8 and 9 suggest that receiver aperture smoothing will be very poor for high integrated-path turbulence levels. This was directly confirmed with large-receiver measurements, as shown in Table IV.

TABLE IV. Typical Receiver Aperture Smoothing Results at 4880 Å

The receiver smoothing factor Ω is the log amplitude variance for a 32 cm receiver, normalized by that for a small (6 mm) receiver.

C_n^2	Ω
3.1×10^{-12}	0.46
7.5×10^{-13}	0.35
5.4×10^{-13}	0.70

III. Transmitter Aperture (Finite Beam) Effects

A. Introduction

The effects of turbulence on finite beams include beam wander, instantaneous beam spread, scintillations, and wavefront distortion. Wander and spread affect mean target-irradiance, and wander and scintillations cause fading. Unfortunately, these phenomena have not been well understood, and theoretical predictions in the literature are characterized by apparent inconsistencies and discrepancies--in some cases due to inadequate definition of the conditions under which they apply.

In this section, we will attempt to remove the discrepancies and unify the predictions. We will then define a related experimental program.

B. Reciprocity

It is physically apparent that beam wander is a geometric-optics phenomenon, while instantaneous spread may be due to either diffraction or multiple refraction by the turbulence. Let us consider a transmitter optic and target point, as in Figure 17a; the conceptual, reciprocal case,[10] involving the point as a coherent source and the transmitter as an imaging or optical heterodyne receiver system, is shown in Figure 17b. It is a consequence of reciprocity that beam wander and spread in the target illumination system are respectively related to image dancing and spread in the reciprocal heterodyne.[11]

In particular, if the beam is nearly diffraction limited but wanders off target due to atmospheric effects, a virtual target-point at the new beam-center will yield a diffraction limited, centered image (or high heterodyne-efficiency) in the reciprocal system; it is clearly implied that the original target point will yield a diffraction limited, non-centered image. This suggests a means of eliminating beam wander through tracking, as discussed in later sections.

The beam-image reciprocity enables us to make use of theoretical descriptions of image behavior in order to investigate finite-beam wander and

spread at the target. The application of reciprocity will also aid in the understanding of target scintillations vs. transmitter aperture diameter, since the phenomena reciprocal to scintillation include "atmospheric modulation noise"[12] or coherent fading in an optical heterodyne, and this has been analyzed.

C. Parameters and Structure Functions

The basic physical parameters in this discussion are:

inner scale of turbulence	ℓ_o
optical diameter	b
strength of turbulence	C_n^2
pathlength (assumed horizontal)	L
optical wavenumber	k

Important quantities defined on these parameters[1] include the wave structure function $D(\rho)$, the phase structure function $D_\phi(\rho)$, and a coherence scale ρ_o, all of which apply at the optic when (conceptually) looking at the point source of Figure 17b. The (asymptotic) behavior of finite beams will depend upon the relative values of ℓ_o, ρ_o, and b, i.e. upon which of the six possible inequalities between these parameters applies in any given case. The corresponding structure functions and ρ_o values are summarized in Table V.

With regard to these structure functions, it should be pointed out that Lutomirski and Yura[10,13] have calculated corrections due to outer scale (L_o) effects, which they have shown to be significant for $\rho \gtrsim 0.1\ L_o$. In particular, at this value of ρ the exponent is closer to 3/2 than 5/3, and since simple image dancing or beam wander corresponds to an exponent of 2, outer scale effects may in some cases lessen the advantage of wander-tracking. Also, if L is not appreciably greater than a critical distance which is outer-scale dependent, then the value of ρ_o, the atmospheric MTF at large ρ, and the heterodyne efficiency (or image resolution) at large apertures are all increased over values computed without this outer-scale correction.

TABLE V. Structure Functions and Coherence Scales for Point Sources[1, 10, 13]

Note: The coherence scale ρ_o is defined such that $D(\rho_o) = 2$.

The pertinent value of separation (ρ) in $D(\rho)$ is $\rho = b$, the optical diameter.

WAVE STRUCTURE FUNCTION D

(1) $\rho_o > b > \ell_o$

$b > \rho_o > \ell_o$

$$D(b) = 1.1\, k^2\, L\, C_n^2\, b^{5/3} \equiv 2 \left(\frac{b}{\rho_o}\right)^{5/3} \tag{4}$$

$$\rho_o = (0.545\, k^2\, L\, C_n^2)^{-3/5} = 1.44\, (k^2\, L\, C_n^2)^{-3/5} \tag{5}$$

(2) $\rho_o < b < \ell_o$

$b < \rho_o < \ell_o$

$$D(b) = 0.62\, L\, k^2\, C_n^2\, b^2\, \ell_o^{-1/3} \equiv 2 \left(\frac{b}{\rho_o}\right)^2 \tag{6}$$

$$\rho_o = (0.309\, Lk^2 C_n^2\, \ell_o^{-1/3})^{-1/2} = 1.80\, (Lk^2 C_n^2\, \ell_o^{-1/3})^{-1/2} \tag{7}$$

(3) $\rho_o < \ell_o < b$

$b < \ell_o < \rho_o$

Structure function not readily available in literature. For completeness, this will be further investigated at a later date.

PHASE STRUCTURE FUNCTION D_ϕ

$D_\phi = D$ when $b >> (L/k)^{1/2}$ (near field) (8)

$D_\phi = \frac{D}{2}$ when $b << (L/k)^{1/2}$ (far field) (9)

These relations apply directly to case (1) above, and we surmise that they apply to case (2). This will be further investigated at a later date.

NOTE: Case (1) obviously has the greatest practical importance.

D. Beam Wander and Spread

There are a number of alternative definitions of beam wander and instantaneous spread.[14-17] If we divide by the path length in order to use an angular description, the spread definitions may alternatively involve the second moment, half-power width, or on-axis irradiance; similarly, the wander definitions include the second moment, and image-dance or angle-of-arrival designations[17] for the reciprocal system. In most cases, the alternative definitions yield similar results which differ only by numerical constants.

In the present discussion, we will invoke the simplest possible definitions in order to clarify breakpoints and asymptotic dependencies; we believe that these results are dimensionally correct, and that any necessary numerical constants may be readily added at a later date.

We point out that, regardless of the definitions used, the mean square total spread angle is the sum of the mean square wander and instantaneous spread angles.

Wander

The simplest definition of image dancing or wavefront angle-of-arrival (tilt) variations is[1,17-19]

$$\Phi^2 = \frac{D_\phi(b)}{k^2 b^2} \quad . \tag{10}$$

Invoking the reciprocity principle, we also utilize this definition to describe beam wander. It will be seen that the results are dimensionally consistent with other treatments in the literature,[15, 16, 18, 20-23] and they will clarify regions of validity of those treatments.

A summary of the mean-square angle subtended by beam wander, as defined by Eq. (10), is given in Table VI. This geometrical optics effect is wavelength independent, and depending upon the relative sizes of b and ℓ_o, is proportional to $b^{-1/3}$ or $\ell_o^{-1/3}$.

TABLE VI. Mean Square Beam-Wander Angle.

(1) $b > \ell_o$

$\ell_o < b < \rho_o$

$$\Phi^2 = 1.1\, L\, C_n^2\, b^{-1/3} \qquad b \gg (L/k)^{1/2} \text{ (near field)} \tag{11}$$

$$= 0.55\, L\, C_n^2\, b^{-1/3} \qquad b \ll (L/k)^{1/2} \text{ (far field)} \tag{12}$$

$\ell_o < \rho_o < b$

Same as above, but beam spread may predominate (see text).

$\rho_o < \ell_o \lesssim b$

No structure function immediately available; beam-spread predominates.

(2) $b < \ell_o$

$b < \rho_o < \ell_o$

$$\Phi^2 = 0.62\, L\, C_n^2\, \ell_o^{-1/3} \qquad \text{(near field)} \tag{13}$$

$\rho_o < b < \ell_o$

Same as above (13)--multiple refractive effects (see beamspread).

$b < \ell_o < \rho_o$

No structure function immediately available; geometrical optics gives above result (13).

Instantaneous Spread

For $b > \rho_o$, the transmitter aperture encompasses a number of (reciprocal) coherence diameters, and diffraction from one such diameter yields the spread:

$$\theta^2 = \frac{1}{(k\rho_o)^2} \qquad (14)$$

The results are summarized in Table VII. Note that for $\rho_o < b < \ell_o$, the multiple refraction from the inner scale is indicated, and the functional dependence is identical to that for beam wander.

TABLE VII. Mean Square Instantaneous Beam-Spread Angle ($b > \rho_o$)

$b > \rho_o > \ell_o$

$$\theta^2 = 0.48\, k^{2/5} L^{6/5} C_n^{12/5} \qquad (15)$$

$\ell_o > b > \rho_o$

$$\theta^2 = 0.31\, L\, C_n^2\, \ell_o^{-1/3} \qquad (16)$$

$b > \ell_o > \rho_o$

No structure function immediately available.

For $b < \rho_o$, there is no simple analytical result for instantaneous spread. However, for $\ell_o < b < \rho_o$, the result is implied in heterodyne tilt-tracking[24] or short-exposure imaging[25] analyses; the reduction in heterodyne efficiency or image resolution which remains after instantaneous image dancing (beam wander) is removed is a direct indication of image smearing (beam spread). In particular, as the aperture is increased, the higher-order or nonlinear wavefront-distortion terms (i.e. in the reciprocal system) become more important, and spreading increases while wander decreases in accordance with Eq. (11). In general, in this regime the short-term spread is smaller than either $(1/k\rho_o)^2$ or the wander angle. This will be discussed further in a later section.

Total Spread, Breakpoints, Asymptotic Behavior

The mean square long-term spread is defined as

$$\theta'^2 = \theta^2 + \Phi^2 \tag{17}$$

If we consider the most important practical case, i.e. negligible inner scale effects ($\ell_o < \rho_o$, b), we may clarify the discussion by constructing an asymptotic diagram of total spread vs. b, showing breakpoints between the various regimes. If we add to the previous definitions the mean square aperture diffraction angle $(kb)^{-2}$, and assume the more interesting case of the near field, we may use Eqs. (11) and (15) to obtain Figure 18. For the particular numerical constants used here (i.e. unity in Eqs. (10) and (14)), the breakpoints are given by

$$\begin{aligned} b_1 &= 0.65\,\rho_o \\ b_2 &= 8.4\,\rho_o \\ b_2/b_1 &= 12.9 \end{aligned} \tag{18}$$

Hence there is always a wander-predominating regime, with an upper-lower breakpoint ratio which is independent of all parameters. Note that for $b >> \rho_o$, the spread is entirely determined by the atmosphere, and is aperture-independent; this may be termed "aperture saturation."

Within this wander-predominating regime, there exists the possibility of reducing long-term spread by cancelling-out beam wander. This cancellation may be achieved by making the outgoing transmitter wave angle (Fig. 17a) correspond to the incoming angle from the target (17b). A reflection off the target may be utilized, and in principle the target need not be cooperative. If such a tracking system is used, then beam wander is eliminated and the broken lines in Figure 18 apply. There is then an optimum aperture for minimum long-term spread, and we note that an inversion of the diagram of Figure 18 is consistent with plots of tilt-tracking heterodyne signal power[24] or short-term image resolution.[25] This will be further discussed below, in the context of mean-target irradiance.

It is of interest also to consider the far-field case. If $b < (L/k)^{1/2}$, the phase structure function is reduced to half the total wave structure function, the other half being comprised of the amplitude structure function, implying substantial scintillations. The beam wander is reduced by a factor of two, and the breakpoints corresponding to (18) are

$$\begin{aligned} b_1 &= 0.99\ \rho_o \\ b_2 &= 1.04\ \rho_o \\ b_2/b_1 &= 1.05 \end{aligned} \qquad (19)$$

Hence, the wander regime essentially disappeared, and instantaneous beam spread is practically a nil consideration.

Note that the requirement $\rho_o >> (L/k)^{1/2}$ is equivalent to requiring $C_n^2 k^{7/6} L^{11/6} << 1$, i.e. that the amplitude scintillations not be saturated.

We point out that the parameter r_o, which appears in analyses of imaging or optical heterodyne performance in turbulence, is simply related to ρ_o:

$$r_o = 2.15\,\rho_o \quad . \tag{20}$$

The intersection of the aperture and atmospheric diffraction asymptotes in Figure 18 occurs at $b = \rho_o$ for our inexact numerical constants and unspecified aperture illumination; r_o simply represents an exact value for the particular case of a uniformly-illuminated aperture.

The relationship (20) is true in either the plane or spherical wave cases, and we note additionally that

$$\frac{\rho_{o\,sph}}{\rho_{o\,pl}} = \frac{r_{o\,sph}}{r_{o\,pl}} = 1.8 \quad . \tag{21}$$

Although the heterodyne analyses were originally carried out for plane wave sources, the results carry over directly to the spherical wave (point source) case which is appropriate for reciprocity reasonings; we merely change the value of ρ_o or r_o accordingly. This is also true of the scintillation analysis in Section F below. Furthermore, our reasonings may be immediately extended to a nonhorizontal path, by utilizing appropriate structure functions and values of ρ_o.

E. Mean Target-Irradiance

The application of reciprocity tells us that the average target-irradiance is one-to-one related to the image resolution or the effective received power P in a heterodyne ($\sim$ SNR). In fact, we expect that $P^{-1} \sim \theta_i^2$. We replot the quantity P, normalized by that for an infinite aperture, in Figure 19 (taken from Ref. 25), and note the consistency with Figure 18. In particular, this tells us that the improvement in near-field mean irradiance which can be obtained with wander-cancellation and an optimum aperture (for any given condition or value of ρ_o) is ≈ 6 dB, relative to that for a very large, static aperture. This occurs at $b = 3.8\,r_o$, where the instantaneous atmospheric beam spread equals the aperture diffraction spread (Figure 18).

Note that if $\rho_o < (L/k)^{1/2}$, the optimum b will not be well in the near field, and the above advantage cannot be obtained. Hence, equivalently,

the amplitude scintillations must be well below saturation for wander-cancellation to be advantageous; this may often be of more practical importance at 10.6 μm than at shorter wavelengths, and will depend upon the other parameters of the situation.

We note that the atmospheric spread and wander angles implicit in the heterodyne analyses and Figure 19 are those deduced from mean on-axis irradiance. This does not exactly agree with our wander definition (Eq. 10). Also, in the heterodyne analyses the optimum tilt-tracking is defined in terms of minimizing the integral of the quadratic phase function over the aperture, which is not exactly equal to cancelling $D_\phi(b)$. However, for practical purposes the differences in these definitions are small.

F. Fading

In the above discussion, we have considered angular wander and spread and their effects on mean target-irradiance. Fluctuations in this irradiance arise due to both wander and scintillations, and are also of great importance. Unfortunately, these finite-beam effects have been poorly understood, and in this section, we will attempt to clarify these considerations.

Scintillation

An apparent contradiction in the theoretical literature is the following. Perturbation (Rytov) scintillation analyses have predicted[27-29] that, for a focused near-field transmitter over a horizontal path, the scintillations decrease arbitrarily as the aperture is made arbitrarily large. However, the application of reciprocity and coherence theory[11,12] results in the prediction of an "atmospheric modulation noise" or coherent fading, which increases asymptotically as b^2.

In a recent report,[30] we speculated that the true conditions for applicability of the Rytov analysis become progressively more severe as the aperture increases; this has now been directly verified by Gochelashvily,[31] who shows that such analyses are valid only for $D_\phi(b) \ll 1$, i.e. $b \ll \rho_o$. Dimensionally,

it was shown in Ref. 30 that this is equivalent to requiring that the point-source or spherical-wave log amplitude variance σ^2 due to scintillations satisfy

$$0.124\, C_n^2 k^{7/6} L^{11/6} = \sigma_s^2 \ll \text{constant X (transmitter Fresnel number)}^{-5/6} \quad (22)$$

Hence, as the turbulence increases, the maximum aperture for which the scintillation reduction will be experienced will decrease; this is consistent with the onset of a further noise mechanism at larger apertures, i.e. coherent fading.

We now express the normalized variance of (linear) irradiance σ_I^2 at the target of Figure 17a following Fried's approximate heterodyne noise analysis:[12]

$$\sigma_I^2 = e^{4 a \sigma_s^2 f(b/r_o)} - 1 \quad , \quad (23)$$

where σ_s^2 is the point-source scintillation above, a is an "aperture smoothing" factor which represents the Rytov prediction of decreased scintillation with increasing aperture, and $f(b/r_o)$ is the coherent fading contribution ($\sim b^2$ for $b \gg r_o$). The situation is summarized in the approximate asymptotic diagram of Figure 20. It is apparent that the optimum transmitter aperture size is of the order of r_o, and that a substantial decrease in target irradiance fluctuations may be achieved providing $r_o \gg (L/k)^{1/2}$. We suspect that the indefinite increase in σ_I^2 which is predicted for increasing b is incorrect and indicates a further breakdown of the theory in the multiple scattering region. This is intuitively apparent, and is supported by measurements in Ref. 30, where it was found that scintillations in this regime ($b \gg r_o$) approached those for a point source.

It is interesting to note that the extreme focus-criticality which is predicted[29] and observed[30] for the smoothing of fluctuations ($b \lesssim r_o$) is consistent with the reciprocal heterodyne viewpoint; this criticality is equivalent to the wavefront-matching requirement between the incoming and local oscillator beams.[32] We also notice that the new (coherent fading) noise mechanism is a manifestation of atmospherically induced beam breakup (Figure 18).

It was pointed out earlier that the requirement $r_c >> (L/k)^{1/2}$ is equivalent to requiring that point-source scintillations be well below saturation. If that is not the case, the scintillation reductions shown in Figure 20 cannot be observed; beam breakup will take over before aperture-smoothing occurs.

We now argue that beam wander (wavefront tilt) has been implicitly removed in the analyses leading to Figure 20, i.e. in Refs. 12, 27-29. Without this removal, a new fading mechanism due to wander needs to be added; the measurements in Ref. 30 indicate that the resultant logarithmic fluctuations may be an order of magnitude more severe than the point-source scintillations! We now consider this point in more detail.

Wander Fading

In a recent analysis, Titterton[33,34] has extended an analysis by Esposito[35] to show that the mean irradiance $\overline{I}$ and irradiance variance σ_I^2 (on the long-term axis) due to wander are given by

$$\frac{\overline{I}}{I_o} = \frac{1}{1 + 2\,\Delta} \tag{24}$$

$$\sigma_I^2 = \frac{4\,\Delta^2}{4\Delta + 1} \tag{25}$$

where I_o is at the instantaneous beam center, and

$$\Delta = \frac{\text{mean-square displacement}}{\text{radius}^2} \sim \frac{\Phi^2}{\theta^2} \quad . \tag{26}$$

Note that for large wander, $\overline{I} \sim \Phi^{-2}$ as expected.

If the aperture diffraction spread is greater than the instantaneous atmospheric spread (Figure 18), we have from Eq. (11):

$$\Delta \sim \frac{1.1\, L\, C_n^2\, b^{-1/3}}{\frac{1}{k^2 b^2}} = \frac{2\, b^{5/3}}{\rho_o^{5/3}} = D(b). \qquad (27)$$

(In Titterton's analysis, the 5/3 exponents are approximated by 2.) Combining this with Eq. (25), we have

$$\sigma_I^2 \sim \frac{4\, D(b)^2}{4D(b) + 1} \quad . \qquad (28)$$

Similarly, at large apertures $\theta^2 = (k\rho_o)^{-2}$ and we have

$$\Delta \sim 2(\rho_o / b)^{1/3} = 2.3\, [D(b)]^{-1/5} \quad , \qquad (29)$$

$$\sigma_I^2 \sim \frac{21\, D^{-2/5}}{9.2\, D^{-1/5} + 1} \quad . \qquad (30)$$

These expressions (28, 30) may be utilized in another asymptotic diagram (Figure 21), where the peak value of $\sigma_I^2(b)$ is a fixed number independent of conditions. If wander cancellation is not employed, this fading mechanism must be added to those shown in Figure 20, as crudely indicated there. The relative height of the wander fading will depend on σ_s^2; measurements have shown[30] an order of magnitude increase in the logarithmic fluctuations due to this mechanism. In future efforts, we will seek more precise quantitative predictions as a function of the independent parameters.

G. Summary

In summary, it is apparent that the successful cancellation of beam wander has two potential advantages:

(1) The mean target irradiance may be improved up to 6 dB over that for a very large aperture

(2) The fluctuations in target irradiance may be very substantially reduced relative to those for a large aperture.

In order to achieve these advantages, the transmitter aperture must be variable in accordance with the value of ρ_o, so that a knowledge of the atmospheric MTF is critical.

H. Further Comments on the Literature

There have unfortunately not been many measurements of wander and spread, and none of scintillations with wander-cancellation. Alcaraz and Livingston[20] have reported a rough corroboration of the range-dependence in Eq. (11), but a poor correlation with C_n^2. It is to be expected that substantial contributions to beam wander will occur due to turbulence scales larger than the outer scale, where C_n^2 is not a meaningful measure. This is especially true for longer-term components.[38]

Kuriger[39] has described a modulation phase technique for measuring wander, and presents some data. Hansen and Madhu[40] have observed and attempted to explain a curious effect involving large image dancing for a retro return relative to a nearby incoherent source; we have not been able to duplicate this effect, and we do not accept the explanation given. This possible anomaly will be investigated further.

Comprehensive wander and spread measurements have been conducted at NRL[16, 41, 42] but, unfortunately, no attempt was made to identify the data in terms of realms of (ℓ_o, b, ρ_o), so that interpretation is difficult. For instance, data at 6328Å ($b >> \rho_o$) are intermixed with data at 10.6 μm ($b < \rho_o$). A high degree of correlation was found between wander at the two wavelengths, which supports the geometrical view of that phenomenon. We believe that these very substantial data can be more usefully interpreted by relating them to ρ_o and (if known) ℓ_o.

I. Physical Viewpoint of Transmitter Aperture Smoothing of Scintillations

In this section, we attempt to lend some insight into the phenomenon of transmitter-aperture smoothing of scintillations ($b < r_o$ in Figure 20), using a heuristic physical argument based on ray optics and interference. The degree of scintillation at any point is determined by the percentage of incident rays

which have relative phase shifts $\gtrsim \pi$.

(1) Within the Focal Spot--Horizontal Case

Consider a near-field source S focused on a receiver plane R at distance L, as in Figure 22. We know that the physical optics solution in a vacuum leads to a finite focal spot at R, and we consider all of the energy, including this diffraction spread, as represented by rays. One such (arbitrary) ray is shown in the figure, and we note that the size of R is determined by the requirement that rays incident at an angle equal to the subtense of S have substantially equal lengths or phases for all points on R (in particular, at both edges of R).

We model the turbulence as consisting of small, weak refractive scatterers giving rise to scattered rays such as the one shown, where the (small) scattering angle is β, and z' is the distance from the scatterer to R.

In order to ensure that the scattered ray cannot interfere with the nonscattered rays, we require

$$k\beta^2 z' \ll 1 \quad . \tag{31}$$

Since $(\beta z')_{max} = R \cdot \frac{L}{kS}$, we rewrite this as

$$k\beta R = k\beta \frac{L}{kS} \ll 1, \quad \beta \ll \frac{S}{L} \quad . \tag{32}$$

This simply manifests the way in which R was established; all non-interfering scattered rays subtend S. Also, we note that interference can occur only for

$$z'/L \lesssim L/kS^2 \tag{33}$$

Hence, as the source Fresnel number is increased, rays which can interfere are restricted to larger scattering angles and a smaller scattering region. Thus for large source apertures, scintillations in the focused spot are drastically reduced.

(2) Within the (Far Field) Spot--Vertical Case

Consider a ray which is scattered near a collimated transmitter, as shown in Figure 23. The scattering is assumed to occur through an angle β at a distance z'' from the source; since the far-field is by definition angularly-resolved, we compare the scattered ray with an unscattered ray to which it is parallel. To ensure no interference, we require

$$k \beta^2 z'' \ll 1 \quad . \tag{34}$$

Since $\beta_{max} = R/L$ within the far field spot, we rewrite this as

$$k z'' \frac{R^2}{L^2} = \frac{k z''}{L^2} \frac{L^2}{k^2 S^2} \ll 1, \frac{z''}{kS^2} \ll 1 \quad . \tag{35}$$

Hence, scattering which occurs within the near field of S will cause no appreciable scintillation, in agreement with theory.[30]

(3) Outside the Focal Spot, at Focal Plane

In this region all rays are the result of scattering, and we expect a high degree of randomization and interference, which is observed.[30] Since the region within R scintillates less as S is increased, by conservation of energy there is then less irradiance appearing outside the spot.

(4) Outside Near Field of Focal Region

Consider a ray which is scattered by a small angle ($S/L \gg \beta \gg R/L$) and bound for a point P outside the focal spot, with a correspondingly significant phase shift and ability to interfere (Figure 24). Outside of the near field of the focal spot, it can overlap the unperturbed rays. Hence, for small transmitter defocusing, scintillations on the target become very substantial.[29, 30]

(5) Multiple Scattering

The above discussion assumes single scattering events, in which

each ray is scattered only once and the basic field is substantially unperturbed. If the scattering is stronger, much of the energy is taken out of R, and the spot is spread with considerable opportunity for interference everywhere.

In this situation, it is not clear that the scintillating patch size is the usual L/kS, although measurements support this covariance scale under these conditions.[30] For an atmospherically spread but substantially confined beam, conservation of energy requires that the covariance must integrate to zero over the cross-section. Thus the patch size cannot increase indefinitely with increasing turbulence as it does in Section II for a point source. When the $(k\rho_o)^{-2}$ atmospheric spread predominates, a larger transmitter may be expected to result in added independence and decreased patch size (perhaps $\sim \frac{L}{kS}$).

Note that as S is increased and unperturbed R is decreased, this mechanism of substantial scattering outside of R is effective at smaller scattering angles. A measure of the effect is the value of $D_\phi(S)$, as per previous discussions of the breakdown of Rytov analyses.

(6) Other Remarks

Beam wander can be represented in this model as occurring due to larger refractive wedges. This effect does not alter the preceding considerations.

Aberrations in the optical system produce unperturbed rays out of R (Figure 25), which can be scattered back into R to interfere and cause scintillations, even in the single-scatter regime. It may be shown that, for scattering e.g. near midpath, interference will occur for scattering angles $\beta \geq \frac{RS}{L}$.

An alternative and more rigorous approach to these heuristic arguments would be to apply a Fourier optical approach, whereby the turbulence is represented in terms of thin phase screens having single spatial frequencies,[36] each of which scatters part of each incident plane wave component into two new (weak) angular components. Alternatively, each can be considered

to scatter part of the unperturbed gaussian-mode energy through these two angles, and the above arguments can be applied in order to determine the possibility for interference or scintillation.[37]

J. Experimental Program

We are now instrumented to demonstrate the cancellation of beam wander through the use of a tracker with a small target retroreflector. Using the reciprocity philosophy, the instantaneous, mean angle of arrival of the reflected energy is matched by the outgoing transmitter wavefront. We have already qualitatively observed that this approach maintains the beam centroid on the target retro.

In order to quantify the results and to explore the relationships discussed in the preceding sections, we will perform measurements as outlined in Table VIII. These experiments will be conducted at 6328Å, with and without wander-cancellation, with a near-field focused transmitter.

TABLE VIII. Finite-Beam Measurements--Target Illumination

Parameters:	Strength of turbulence (C_n^2, ρ_o)
	Inner scale (ℓ_o)
	Aperture size (b)
	Range (L)
Measurements:	Microthermal C_n^2
	Turbulence spectrum for ℓ_o
	Target mean irradiance
	Target irradiance fluctuation statistics, variance, and power spectrum

---

K. Angular Beam Dithering

During initial experiments with the tracking system, a loop instability resulted in a small, rapid (1 kHz) angular dithering of the beam. This

resulted in a substantial washing-out of visually observed scintillations. The explanation for this is that turbulence structure near the transmitter results in a scintillation pattern which dithers with the beam, and this component of the total pattern is hence being dithered faster than eye-response. The small dither angle can be achieved electro-optically at e.g. microwave rates,[43] and it is suggested that this effect might be useful since it would translate much of the scintillation power spectrum to GHz frequencies and hence out of the necessary response range of many atmospheric systems. We will pursue this further.

IV. The Effects of Turbulence Intermittency

As discussed in the preceding report,[3] the macroscale-intermittency or nonuniform development of turbulence which is often observed may be expected to have substantial and hitherto unexplored effects on scintillations. These effects may include (1) inner scale influences due to the confinement of strong turbulence to narrow regions along the path, and (2) large statistical variations in scintillation levels due to the poor relationship between any instantaneous path-realization and long-term or ensemble average conditions. The usual theoretical expressions, which relate scintillations and turbulence in terms of long-term average quantities, may be invalidated by (1) and will certainly mask short-term deep fades implied by (2). Also, (2) relates to the large data spread which is usually observed in scintillation experiments.

In the following discussion, we analyze the first effect and show that it will normally not be substantial, and then we refine our definition of the statistical problem represented by the second effect. Our further work will involve the theoretical and experimental investigation of this latter topic.

A. Propagation Through a Turbulent Slab - Inner Scale Effects

The simplest model of turbulence intermittency is that of discrete slabs. Consider a large transmitter propagating a quasi-plane-wave over a pathlength L, as in Figure 26. The turbulence is confined to a slab of length d, located at distance b from the receiver. The turbulence within the slab is statistically uniform with a strength C_n^2, and fits the Kolmogorov spectral model:[1]

$$\Phi_n(\kappa) = 0.033\, C_n^2\, \kappa^{-11/3}\, e^{-\kappa^2/\kappa_m^2}, \tag{36}$$

where Φ_n is the refractive index spectrum, κ is the spatial wavenumber, and $\kappa_m = 5.92/\ell_o$. The log amplitude variance of the received beam is given by[1, 44]

$$\sigma^2 = 2\pi^2 k^2 d \int_0^\infty F(\kappa)\, \Phi_n(\kappa)\, \kappa\, d\kappa, \tag{37}$$

where $F(\kappa)$ is the appropriate filter function for the path under consideration. DeWolf[44] has given $F(\kappa)$ for the path of Figure 26 as

$$F(\kappa) = 1 - \frac{\sin\left[(b+d)\,\kappa^2/k\right] - \sin\left[b\kappa^2/k\right]}{\kappa^2 d/k} \quad . \tag{38}$$

Using (38) and (36) with (37), we have

$$\sigma^2 = 2\pi^2(0.033)C_n^2 k^2 d\int_o^\infty d\kappa\ \kappa^{-8/3} e^{-\kappa^2 \ell_o^2/(5.92)^2}\left[1 - \frac{\sin\left[(b+d)\,\kappa^2/k\right] - \sin\left[b\kappa^2/k\right]}{\kappa^2 d/k}\right] \tag{39}$$

In order to check for consistency with well known results, we let $b \to 0$ and $d \to L$ in Eq. (39):

$$\sigma^2 = 2\pi^2 k^2 L\int_o^\infty \kappa\Phi_n(\kappa)\left[1 - \frac{k}{L\kappa^2}\sin\left(\frac{L\kappa^2}{k}\right)\right] d\kappa \tag{40}$$

This is equivalent to Eq. (T1) in Ref. 1.

In order to carry out the integration in Eq. (39), we let $y = \kappa^2$:

$$\sigma^2 = \pi^2(0.033)C_n^2 k^2 d\int_o^\infty dy\ y^{-11/6} \exp\left\{\frac{-y\ell_o^2}{5.92^2}\right\}\left[1 - \frac{\frac{\sin(b+d)y}{k} - \frac{\sin by}{k}}{\frac{yd}{k}}\right] \tag{41}$$

This yields

$$\sigma^2 = \pi^2 (.033) C_n^2 k^2 d \left\{ \Gamma(-5/6) \left(\frac{\ell_o^2}{5.92^2} \right)^{5/6} - \frac{\frac{k}{d} \Gamma\left(-\frac{11}{6}\right) \sin\left[-\frac{11}{6} \tan^{-1}\left(\frac{\frac{b+d}{k}}{\ell_o^2/5.92^2} \right) \right]}{\left[\left(\frac{\ell_o^2}{5.92^2} \right)^2 + \left(\frac{b+d}{k} \right)^2 \right]^{-11/12}} \right.$$

$$\left. + \frac{\frac{k}{d} \Gamma\left(-\frac{11}{6}\right) \sin\left[-\frac{11}{6} \tan^{-1}\left(\frac{b/k}{\ell_o^2/5.92^2} \right) \right]}{\left[\left(\frac{\ell_o^2}{5.92^2} \right)^2 + \left(\frac{b}{k} \right)^2 \right]^{-11/12}} \right\} \qquad (42)$$

Noting that $\Gamma\left(-\frac{11}{6}\right) = -\frac{6}{11}\Gamma(-5/6)$, this becomes

$$\sigma^2 = 0.326 C_n^2 k^2 d \Gamma\left(-\frac{5}{6}\right) \left\{ \left(\frac{\ell_o^2}{5.92^2} \right)^{5/6} + \frac{6}{11} \frac{k}{d} \left[\sin\left[-\frac{11}{6} \tan^{-1}\left(\frac{\frac{b+d}{k}}{\ell_o^2/5.92^2} \right) \right] \right] \right.$$

$$\cdot \left[\left(\frac{\ell_o^2}{5.92^2} \right)^2 + \left(\frac{b+d}{k} \right)^2 \right]^{11/12} - \frac{6}{11} \frac{k}{d} \left[\sin\left[-\frac{11}{6} \tan^{-1}\left(\frac{b/k}{\ell_o^2/5.92^2} \right) \right] \right]$$

$$\left. \left[\left(\frac{\ell_o^2}{5.92^2} \right)^2 + \left(\frac{b}{k} \right)^2 \right]^{11/12} \right\} \qquad (43)$$

For $b \ll d$ and $b/k \ll \ell_o^2$ this expression reduces to (T4) and (T5) of Ref. 1, for $d/k\ell_o^2 \begin{pmatrix} >> \\ << \end{pmatrix} 1$ respectively.

We are most interested in a fairly small value of d at various values of b, and the extent to which the inner scale affects results. We arbitrarily chose $k = 1.2 \times 10^7 m^{-1}$ ($\lambda \approx 5200$ Å), and let ℓ_o range from 3 to 30 mm, such that the corresponding values of $\ell_o^2 k$ range from 108 m to 10.8 km. The results are given in Table IX. We note that, for d = 11m, the inner scale effects are substantial at b = 100m but much less at b = 1 km.

Since the scintillations are strongest for slabs furthest from the receiver, where inner scale effects are minimal, it may be expected that the <u>average</u> effects of the inner scale over a long path are not great. We now derive a good approximation to Eq. (43) which is valid for most cases of interest and for which the inner scale drops out.

TABLE IX. Values of σ^2/C_n^2 from Eq. (43). k is taken as 1.2×10^7 m^{-1}.

b(m)	d(m)	ℓ_o(cm)	σ^2/C_n^2 ($m^{2/3}$)
100	11	0.3	4.9×10^{10}
		0.9	3.1
		1.2	2.3
		2.1	9.0×10^9
		3.0	3.4
500	11	0.3	2.0×10^{11}
		0.9	1.7
		1.2	1.5
		2.1	1.0
		3.0	7.0×10^{10}
1000	11	0.3	3.6×10^{11}
		0.9	3.3
		1.2	3.0
		2.1	2.4
		3.0	1.9
1000	100	0.3	3.4×10^{12}
		0.9	3.1
		1.2	2.9
		2.1	2.3
		3.0	1.9

Referring to Eq. (43), let us assume that $b >> \ell_o^2 k$. We thus have

$$\sigma^2 \approx 0.326\, C_n^2 k^2 d \Gamma\left(-\frac{5}{6}\right)\left\{\left(\frac{\ell_o^2}{5.92^2}\right)^{5/6} + \frac{6}{11}\,\frac{k}{d}\left[\left[\sin\left(\frac{-11\pi}{12}\right)\right]\left[\frac{b+d}{k}\right]^{11/6} - \left[\sin\left(-\frac{11\pi}{12}\right)\right]\left[\frac{b}{k}\right]^{11/6}\right]\right\}$$

$$\approx 0.31\, C_n^2 k^{7/6}\left[(b+d)^{11/6} - b^{11/6}\right]. \qquad (44)$$

As a further approximation, we may require $b >> d$, and write

$$\sigma^2 = 0.57\, C_n^2\, d\, k^{7/6}\, b^{5/6}\,, \qquad (45)$$

which is the central result of this section. We note that the dependence on the inner scale has vanished in this approximation, even though d may be $< \ell_o^2 k$, and the dependence on b is clear. In Table X, we compare results calculated from Eq. (45) with those from the complete expression (43). The approximation is seen to be good even for $b \sim \ell_o^2 k$.

We may write Eq. (45) in a more useful form by recognizing that the average C_n^2 over the path (equal to the long-term average measured at a point) is

$$\overline{C_n^2} = C_n^2\, d/L\,, \qquad (46)$$

where L is the total path length. We thus have

$$\sigma^2 = 0.57\ \overline{C_n^2}\ k^{7/6}\ b^{5/6}\ L\ . \qquad (47)$$

TABLE X. Values of σ^2/C_n^2 from Eqs. (45) and (43). k is taken as $1.2 \times 10^{-7} m^{-1}$ and ℓ_o as 3 mm, such that $k\ell_o^2 = 108m$.

b(m)	d(m)	σ^2/C_n^2 ($m^{2/3}$) (Eq. 43)	σ^2/C_n^2 ($m^{2/3}$) (Eq. 45)
100	1	4.3×10^{9}	4.8×10^{9}
	11	4.9×10^{10}	5.3×10^{10}
	51	2.7×10^{11}	2.5×10^{11}
	101	6.3×10^{11}	4.9×10^{11}
	200	1.6×10^{12}	9.6×10^{11}
500	1	1.8×10^{10}	1.8×10^{10}
	11	2.0×10^{11}	2.0×10^{11}
	51	9.5×10^{11}	9.4×10^{11}
	101	1.9×10^{12}	1.9×10^{12}
	200	4.2×10^{12}	3.7×10^{12}
1000	1	3.2×10^{10}	3.3×10^{10}
	11	3.6×10^{11}	3.6×10^{11}
	51	1.7×10^{12}	1.7×10^{12}
	101	3.4×10^{12}	3.3×10^{12}
	200	7.0×10^{12}	6.6×10^{12}

In order to obtain the long-term average of scintillations, we calculate the average of Eq. (47) over all values of b such that $0 \leq b \leq L$. This corresponds to an equal probability for all possible positions of the slab along the path. The result is

$$\sigma^2 = 0.31\ \overline{C_n^2}\ k^{7/6}\ L^{11/6}\ , \qquad (48)$$

which is the well known expression for a plane wave in uniform turbulence.[1] Since Eq. (47) does not involve the inner scale, we expect this result.

This result, that the inner scale has only a small effect on long-term average scintillations, even though the turbulence regions are much less than $\ell_o^2 k$, may be explained as follows: the inner scale has a substantial influence only for slabs near the receiver, but those slabs in turn give rise to a relatively small degree of scintillation and hence are weakly weighted in the averaging process. The approximation is within 5% for L = 1 km, ℓ_o = 3mm, and d = 1m, as determined from a comparison of Eq. (48) with a true path-averaging of Eq. (43).

We thus conclude that the results of long-term measurements of σ^2 vs C_n^2 will not be appreciably affected by such intermittencies, although such a statement was not obvious before detailed analysis. However, there is clearly a mechanism for significant short-term fluctuations in these quantities, and this will be discussed further in the next section.

B. Further Definition of the Intermittency Statistical Problem

In the preceding report on this program,[3] we have discussed the treatment of finite-time-average measurements of scintillations (log amplitude variance) and microthermal fluctuations at a point (C_n^2) as random variables. We denote these discrete random variables or measurement samples as (x_τ, y_τ) in order to state the problem in a completely abstract way. The physical definitions are

$$x_\tau = C_n^2(\tau) = \text{const. } x \frac{1}{\tau} \int_o^\tau (\Delta T(t))^2 \, dt \tag{49}$$

$$y_\tau = \sigma^2(\tau) = \text{const. } x \frac{1}{\tau} \int_o^\tau \ell^2(t) \, dt \tag{50}$$

where τ is the averaging time, $\Delta T(t)$ denotes the differential temperature fluctuations, and $\ell(t)$ denotes the log amplitude scintillations. For $\tau >>$ decorrelation times, x and y become normally distributed.

There are two types of well-known statistical techniques which may be applied to x and y:

(1) the convergence of either one <u>separately</u> to a mean can be analyzed vs. the averaging time τ and the power spectrum or autocorrelation.[45]

(2) A linear or nonlinear regression analysis may be applied <u>between</u> x and y, with resultant confidence intervals and correlation coefficients.[16,46]

We now suggest theoretical and experimental extensions of these considerations, as follows:

(3) What can be said apriori concerning the statistical relationship between x_τ and y_τ, including data spread or confidence intervals, and correlation coefficients, given a theoretical relationship between related quantities ?

(4) How does this relationship behave as a function of averaging time τ ?

As a corollary, what statistical properties of the relevant physical variables are needed for meaningful answers to the above questions ?

To describe the theoretical relationship referred to in item (3) above, we associate with the point quantity $\Delta T(t)$ a spatial quantity $\Delta T(z)$, where z is the optical pathlength variable ($0 \leq z \leq L$). If we assume the Taylor hypothesis,[1] and the wind happens to be along the path, these two quantities are simply-related:

$$\Delta T(t) = \Delta T(z/v) \quad , \tag{51}$$

where v is the wind velocity. In general, however, the macroscale intermittency may not be assumed to be isotropic; that is, the turbulence regions will not necessarily have equal dimensions along and perpendicular to the wind direction.

We now suppose that some particular realization of the path is frozen, i.e., that the nonuniform turbulence field is invariant. From the results of the preceding section, we drop inner scale effects and write for a nonuniform path:[1]

$$y_\infty = \sigma^2 (\tau = \infty) = \int_o^L f(z)\, C_n^2 (\tau = \infty, z)\, dz \quad , \tag{52}$$

i.e.

$$y_\infty = \text{const.} \times \int_o^L f(z)\, \Delta T^2 (\tau = \infty, z)\, dz, \tag{53}$$

where $f(z)$ is a weighting function. Since it is not practical to know the mean-square temperature fluctuations along the path, these expressions are not directly useful.

We therefore let the overall turbulence structure evolve, and assume stationarity in the long-term statistics. To the extent that this evolution is slow compared to the actual temperature and log amplitude fluctuations, we may utilize a finite τ in Eqs. (52, 53), where τ is intermediate to the fluctuation and evolution time scales respectively. It would appear that, given appropriate statistics of $C_n^2 (\tau, z)$--e.g., the z-correlation function and temperature power spectrum--the above questions can be answered. The integral relationship clearly indicates less spread in y than in x.

C. Disparate Time Scales in Random Processes

As a further attempt to define the problems posed by intermittency, we consider the following. Suppose that the random process x(t) is made up of the product of two processes:

$$x(t) = x_1(t)\, x_2(t) \quad , \tag{54}$$

where the frequency scales involved in the two sub-processes are highly disparate, and the higher-frequency process has zero mean (Figure 27). For example, suppose that the power spectrum of x_1 ranges from 10 to 1000 Hz, while that of x_2 ranges from 0 to 10^{-1} Hz. Since the two are multiplicative, the spectrum of x(t) is at the higher frequencies, with low-frequency sidebands on the x_1 components (Figure 28).

The power spectrum and autocorrelation function of x do not appreciably evidence the presence of the low-frequency multiplier, x_2. However, averaging-time considerations such as those reviewed in Ref. 45 will be invalid, and the overall random process appears nonstationary in the short term. This breakdown of the methods of Ref. 45 is physically obvious, since any short-term attempt to estimate e.g. the mean of x^2 will be invalidated by long-term trends; the formal breakdown of the theory is not as immediately apparent.

In order to avoid these difficulties, we may deal instead with the random variable $x^2(t)$. The low frequency components in x_2 will then appear directly in the power spectrum and autocorrelation function (Figures 29 and 30). For example, for any finite-time estimate of $\overline{x^2}$, we may write

$$\overline{x_\tau^2} = \overline{x^2} + f_1 + f_2 \tag{55}$$

where the additive terms f_1 and f_2 represent the low and high frequency contributions to the error, respectively. These are of course random quantities, with $f_1 \gg f_2$.

The low-frequency multiplying function $x_1(t)$ represents the effects of intermittency. In one model, it consists of a simple two-level function.[47] In general, its probability distribution is of interest; the distribution of x_2 or ΔT is understood.[48] This separation of the temperature function into two frequency or time scales may be usefully applied to the considerations of the preceding section. We will of course continue to refine our theoretical statement of this problem.

D. Experimental Approach

Our field site has been shortened to a uniform path on the order of one mile in length, and restored to a point-transmitter, point-receiver configuration. The microthermal and optical (4880Å and 10.6 μm) instrumentation is being adapted for digital computer processing of analog fm tape recordings of the raw data ($\Delta T(t)$ and $\ell(t)$). This facility is independent of that being utilized in the finite-beam and wander-cancellation work.

The first experiments will consist of (x, y) regression determinations vs. τ, which will be related to the power spectra of ΔT and ℓ. Further efforts may then involve the measurement of the z-correlation of C_n^2, using two or more microthermal systems with variable spacings between the systems, and a second such system is currently under construction. This correlation measurement is equivalent to determining an experimental model of the macroscale intermittency of the turbulence.

In accordance with the preceding section, it may be of interest to treat the square of $\Delta T(t)$, to single out the low-frequency portion $\Delta T(t)$ and measure its probability distribution, and to measure the statistical and spectral properties of the squared quantity. This may be readily achieved on the digital processor.

V. Publications

The following paper is to be published:

J. R. Kerr and J. R. Dunphy, "Experimental Effects of Finite Transmitter-Apertures on Scintillations," J. Opt. Soc. Am., February, 1973.

The following paper will be delivered at the 1973 Spring Meeting of the Optical Society of America, Denver, Colorado:

J. R. Dunphy and J. R. Kerr, "Scintillation Measurements for Large Integrated-Path Turbulence." A written version of this paper will be prepared for publication in the near future.

VI. References

1. R. S. Lawrence and J. W. Strohbehn, Proc. IEEE 58, 1523 (1970).

2. J. Richard Kerr, J. Opt. Soc. Am. 62, 1040 (1972).

3. "Propagation of Multiwavelength Laser Radiation through Atmospheric Turbulence," RADC-TR-72-288, October 1972, Rome Air Development Center.

4. W. P. Brown, Jr., J. Opt. Soc. Am. 62, 966 (1972).

5. D. A. deWolf, "Strong Irradiance Fluctuations in Turbulent Air: Plane Waves," preprint of article submitted to J. Opt. Soc. Am., November 1972. See also J. Opt. Soc. Am. 62, 730A (1972).

6. Note that Eq. (T13) of Ref. 1 has an incorrect coefficient. The correct value is 2.24.

7. Wyngaard, J. C., Izumi, Y., and Collins, S.A., Jr., J. Opt. Soc. Am. 61, 1646 (1971).

8. R. H. Kleen and G. R. Ochs, J. Opt. Soc. Am. 60, 1695 (1970).

9. D. A. deWolf, J. Opt. Soc. Am. 59, 1455 (1969).

10. R. F. Lutomirski and H. T. Yura, Appl. Optics 10, 1652 (1971).

11. D. L. Fried and H. T. Yura, J. Opt. Soc. Am. 62, 600 (1972).

12. D. L. Fried, J. Quantum Electr. QE-3, 213 (1967).

13. R. F. Lutomirski and H. T. Yura, J. Opt. Soc. Am. 61, 482 (1971).

14. Z. I. Feizulin and Y. A. Kratsov, Izv. VUZ Radiofizika 10, 68 (1967).

15. D. A. deWolf, "Effects of Turbulence Instabilities on Laser Propagation." Technical reports RADC-TR-72-32 (January 1972) and RADC-TR-72-204 (July 1972).

16. J. A. Dowling and P. M. Livingston, "The Behavior of Focused Beams in Atmospheric Turbulence: Measurements and Comments on the Theory," preprint, November, 1972.

17. L. R. Zintsmaster and S. A. Collins, Jr., "Angle of Arrival Calculations at 10.6 microns." Technical report RADC-TR-71-124 (June 1971).

18. V. I. Tztarski, Propagation of Waves in a Turbulent Atmosphere, Nauka, Moscow, 1967.

19. C. E. Coulman, Solar Physics 7, 122 (1969). Also see C. E. Coulman, J. Opt. Soc. Am. 56, 1232 (1966).

20. E. C. Alcaraz and P. M. Livingston, Proc. Electro-Optical Systems Design Conference-West, May 18-20, 1971, Anaheim, Calif., pp. 76-80.

21. A. D. Varvatsis and M. I. Sancer, Canadian J. of Phys. 49, 1233 (1971).

22. T. Chiba, Appl. Optics 10, 2456 (1971).

23. A. S. Gurvich, M. A. Kallistratova, and N. S. Time, Izv. VUZ Radiofizika 11, 1360 (1968).

24. D. M. Chase, J. Opt. Soc. Am. 56, 33 (1966).

25. D. L. Fried, J. Opt. Soc. Am. 56, 1372 (1966).

26. D. L. Fried, Proc. IEEE 55, 57 (1967).

27. A. Ishimaru, Radio Science 4, 295 (1969).

28. D. L. Fried and J. B. Seidman, J. Opt. Soc. Am. 57, 181 (1967).

29. J. R. Kerr and R. Eiss, J. Opt. Soc. Am. 62, 682 (1972).

30. J. R. Kerr and J. R. Dunphy, "Experimental Effects of Finite Transmitter-Apertures on Scintillations," to be published in J. Opt. Soc. Am., February, 1973. See also J. R. Kerr, "Multiwavelength Laser Propagation Study," Final Report, ONR Contract N00014-68-A-0461-0001, July 1972.

31. K. S. Gochelashvily, "Focused Irradiance Fluctuations in a Turbulent Medium," preprint, P. N. Lebedev Physical Institute, Academy of Sciences of the USSR, Moscow, 1971.

32. A. E. Siegman, Appl. Optics 5, 1588 (1966).

33. P. J. Titterton, "Power Reduction and Fluctuations Caused by Narrow Laser Beam Motion in the Far Field," preprint, September 1972.

34. P. J. Titterton, "Combined Turbulence Effects on Narrow Light Beams Directed Upward through the Atmosphere," paper to be given at 1973 Spring OSA Meeting, Denver, Colorado, March, 1973.

35. R. Esposito, Proc. IEEE 55, 1533 (1967).

36. R. W. Lee and J. C. Harp, Proc. IEEE 57, 375 (1969).

37. These ideas are due to Prof. Gail A. Massey of the Oregon Graduate Center.

38. G. R. Ochs and R. S. Lawrence, J. Opt. Soc. Am. 59, 226 (1969).

39. W. L. Kuriger, Appl. Optics 10, 2462 (1971).

40. J. P. Hansen and S. Madhu, Appl. Optics 11, 233 (1972).

41. H. Shenker, J. A. Dowling, and J. A. Curcio, "Propagation of Focused Laser Beams," Proc. Electro-Optical Systems Design Conference-West, May 18-20, 1971, Anaheim, Calif., pp. 67-75.

42. J. A. Dowling, J. A. Curcio, and H. Shenker, "The Propagation of Focused Laser Beams through Atmospheric Turbulence," paper 2.7, 1971 Conference on Laser Engineering and Applications, Wash., D.C. June 2-4, 1971.

43. J. R. Kerr, J. Quantum Electr. QE-2, 21 (1966).

44. D. A. deWolf, Radio Science 2, 1513 (1967).

45. P. L. Hunt and S. A. Collins, Jr., "Averaging Times for Atmospherically Degraded Light Beam Measurements," Paper W0-18, Optical Society of America Annual Meeting, October 17-20, 1972, San Francisco, California.

46. J. S. Bendat and A. G. Piersol, Measurement and Analysis of Random Data, Wiley and Sons, New York, 1966.

47. R. S. Lawrence, G. R. Ochs, and S. F. Clifford, J. Opt. Soc. Am. 60, 826 (1970).

48. R. W. Stewart, J. R. Wilson, and R. W. Burling, J. Fluid Mech. 41, 141 (1970).

VII. Figures

1. Experimental log amplitude variance vs. time of day.

   (X) 4880Å on September 14, 1972

   (o) 10.6 μm on September 14, 1972

   (.) 4880Å on August 29, 1972

   The weather was clear except for a trace of ground fog from 0600-0700 on September 14. During the neutral period of typically 0700-0800, the turbulence was poorly developed.

2. Log amplitude variance at 10.6 μm vs. strength of turbulence at 1.8 m height. The data points include several clear days of operation.

3. Same as Figure 2, for 4880 Å.

4. Experimental vs. theoretical (Rytov) log amplitude variance for 10.6 μm. The abscissa is corrected for beam refraction and earth curvature effects. The line indicates the ($\sigma_E^2 = \sigma_T^2$) condition.

5. Same as Figure 4, for 4880 Å. The equation of the linear regression line is

$$\log_{10}\sigma_E^2 = (-0.22) - (0.48)\log_{10}\sigma_T^2 \quad ,$$

   with a correlation coefficient of 0.78.

6. Experimental variances at 4880 Å vs. those at 10.6 μm. The line represents a $k^{7/6}$ dependence.

7. Transverse log amplitude covariance length vs. strength of turbulence. The experimental and theoretical (Rytov) values are for 4880 Å (X, ———) and 10.6 μm (0, ----).

8. Normalized covariance curves for 10.6 μm. The normalizing quantity $C_l(0)$ is identical to σ_E^2, and the 1/e points are indicated. The broken line represents the theoretical (Rytov) function.

Curve	C_n^2
A	4.2×10^{-15}
B	3.6×10^{-13}
C	5.9×10^{-13}
D	3.2×10^{-12}

9. Same as Figure 8, for 4880 Å.

Curve	C_n^2
A	4.5×10^{-15}
B	3.8×10^{-13}
C	6.3×10^{-13}
D	3.4×10^{-12}

10. RMS scintillation spectra at 10.6 μm for the C_n^2 values of Figure 8. The 1/e frequencies are indicated.

11. Same as Figure 10, with the ordinate squared and weighted by the frequency.

12. RMS scintillation spectra at 4880 Å for the C_n^2 values of Figure 9.

13. Same as Figure 12, with the ordinate squared and weighted by the frequency.

14. Linear (left) and log (right) irradiance scintillations at 4880 Å. The pictures from top to bottom represent C_n^2 values A-D respectively of Figure 9. The abscissa is 0.2 sec/cm and the ordinate for the log signal is one decade of irradiance per cm. The linear baseline is one cm up from the bottom of each frame, and the log baseline is indefinite and not pertinent.

15. Same as Figure 14, for 10.6 μm. The turbulence levels are those of Figure 8.

16. Cumulative probability distributions for log irradiance.

Curve	Wavelength	C_n^2
A	4880Å	4.5×10^{-15}
B	4880Å	3.4×10^{-12}
C	10.6 μm	4.2×10^{-15}
D	10.6 μm	3.2×10^{-12}

For curve B, the abscissa should be multiplied by 3.3. The broken curve represents a Rayleigh amplitude distribution.

17. Illustration of the application of reciprocity.

    (a) Target illumination system
    (b) Reciprocal (conceptual) heterodyne receiver or imaging system

18. Asymptotic diagram of total (long term) angular beam spread θ'^2 vs. transmitter aperture b. The mechanisms which predominate for various regions of (b/ρ_o) are indicated. The broken lines refer to behavior with beam wander cancelled out.

19. Mean target irradiance, normalized by that for a very large aperture, as a function of aperture (after Ref. 25).

20. Asymptotic diagram of the logarithm of the normalized irradiance variance vs. aperture. The fading mechanisms which predominate for various regions of (b/r_o) are indicated.

21. Asymptotic diagram of the logarithm of the normalized irradiance variance vs. aperture, for beam wander alone.

22. Illustrating turbulence scattering within the focal spot R of a near-field, focused transmitter S at distance L. The scatterer is located at a distance z' from R, and the scattered ray is at the small angle β with respect to the original ray.

23. Illustrating turbulence scattering near the transmitter for a far-field, collimated transmitter. The scattering occurs at distance z'' from the transmitter, through a small angle β.

24. Illustrating a ray which is scattered out of the focal spot in Figure 22, which can interfere with unperturbed rays in the far field of R.

25. Illustrating scattering into R from an unperturbed ray out of R. The unperturbed ray arises due to aberrations or defocusing. The aberrated ray is at an angle γ with respect to the optical axis, and the scatterer

shown is at midpath with a scattering angle β.

26. Plane wave propagation through a slab of uniform turbulence, representing an idealization of turbulence intermittency.

27. Illustration of random process made up of the product of fast and slow subprocesses.

28. Power spectra of the processes of Figure 27.

29. Square of the random process (x) of Figure 27.

30. Power spectrum of the process of Figure 29.

Figure 1

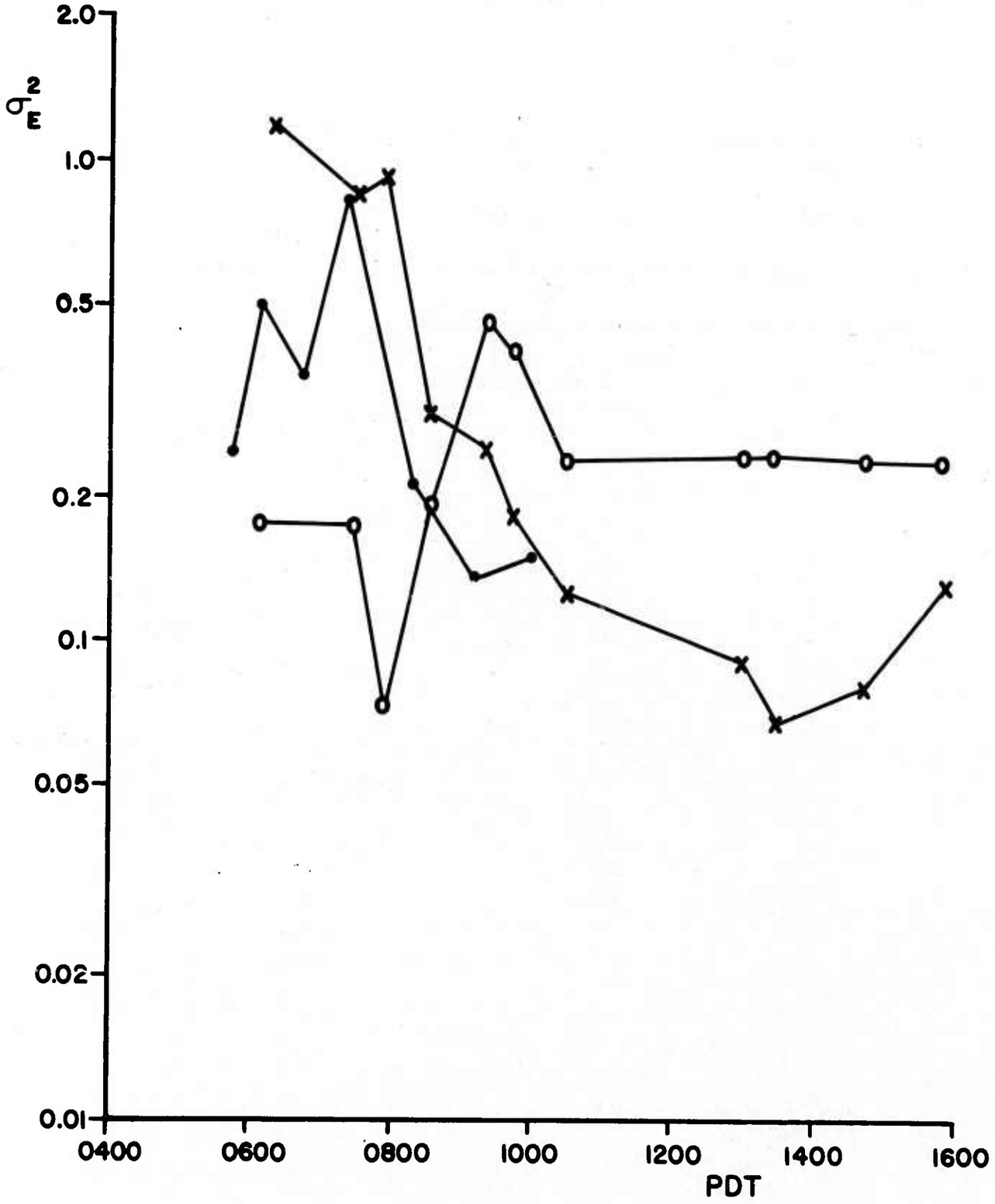
2.0
1.0
0.5
0.2
0.1
0.05
0.02
0.01
σ_E^2
0400
0600
0800
1000
1200
1400
1600
PDT

Figure 2

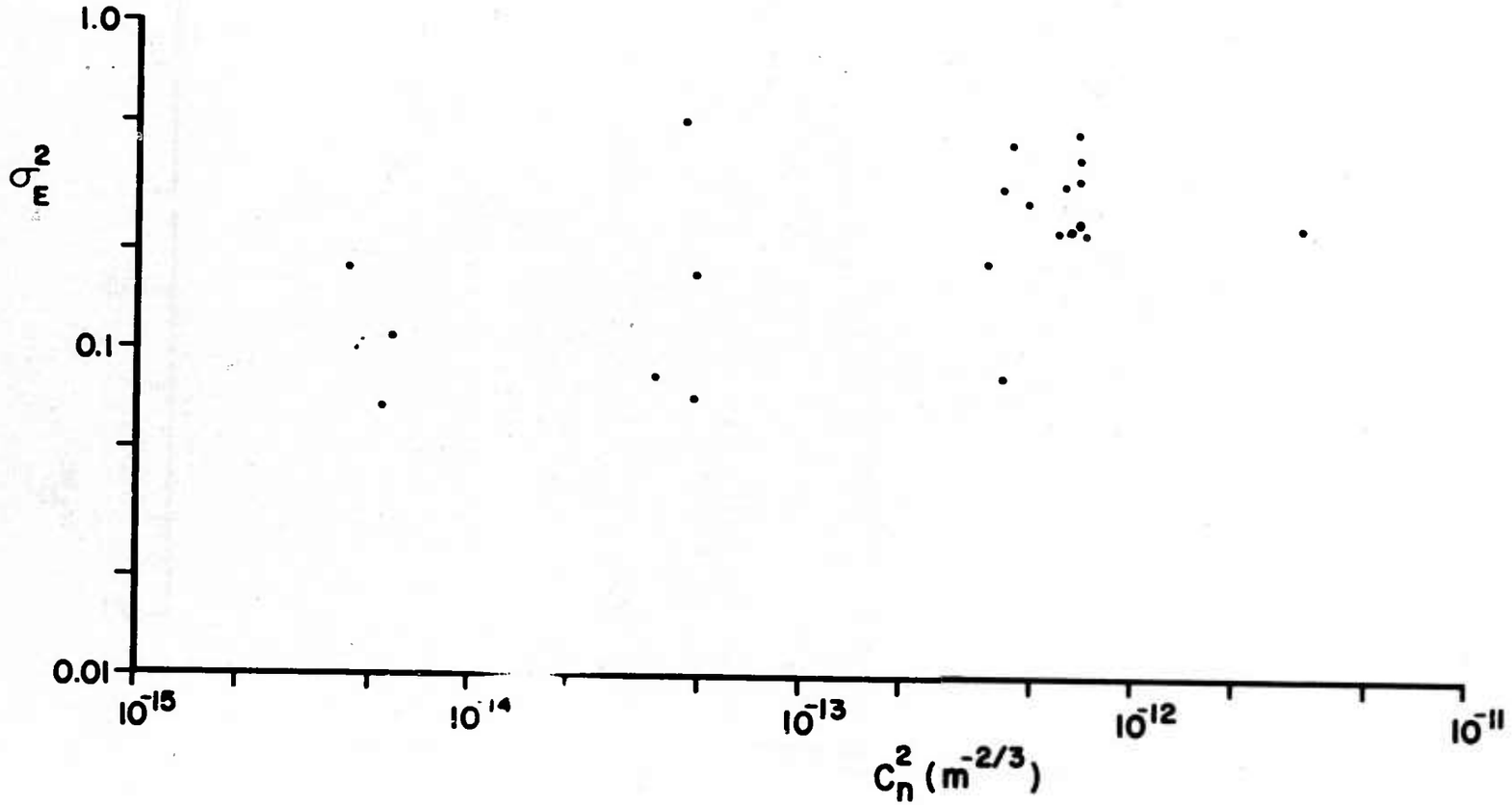

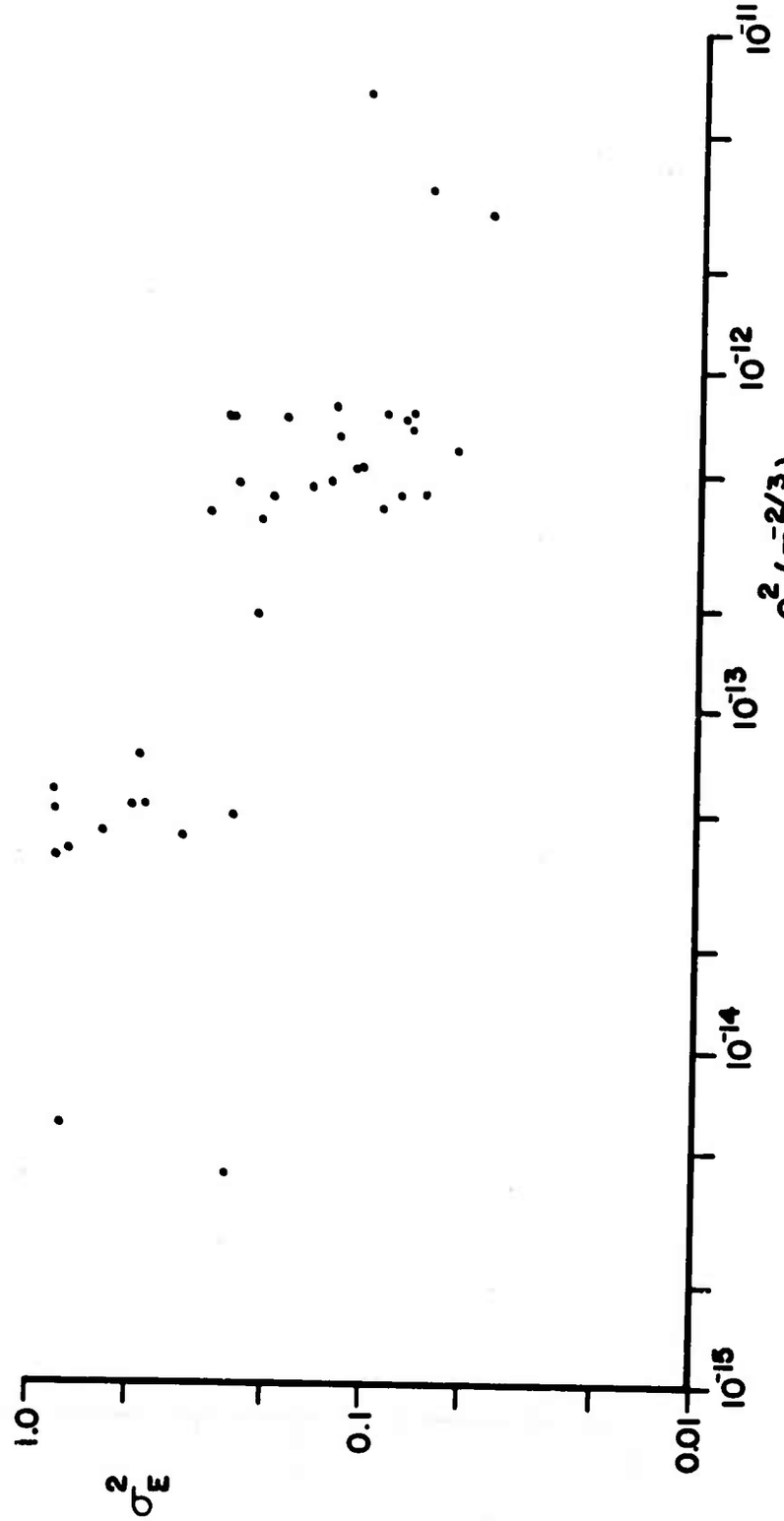

Figure 3

Figure 4

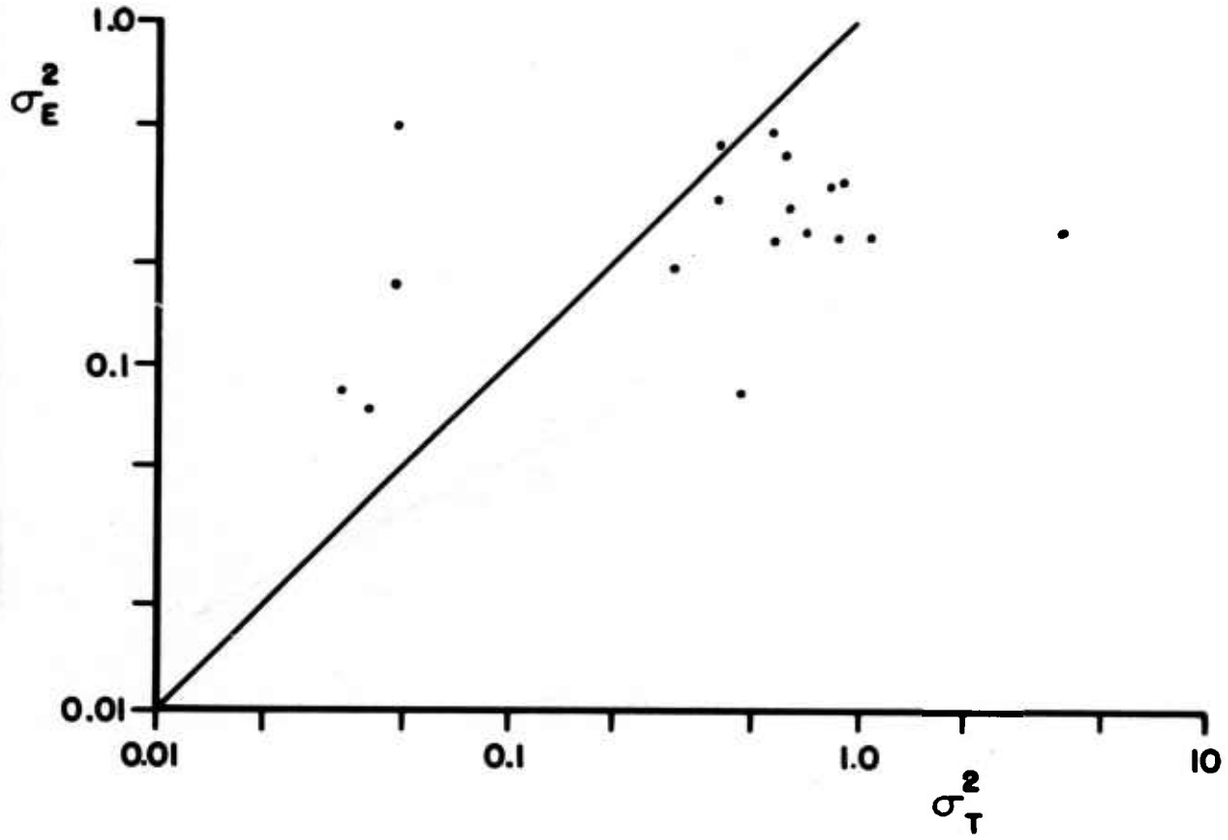

Figure 5

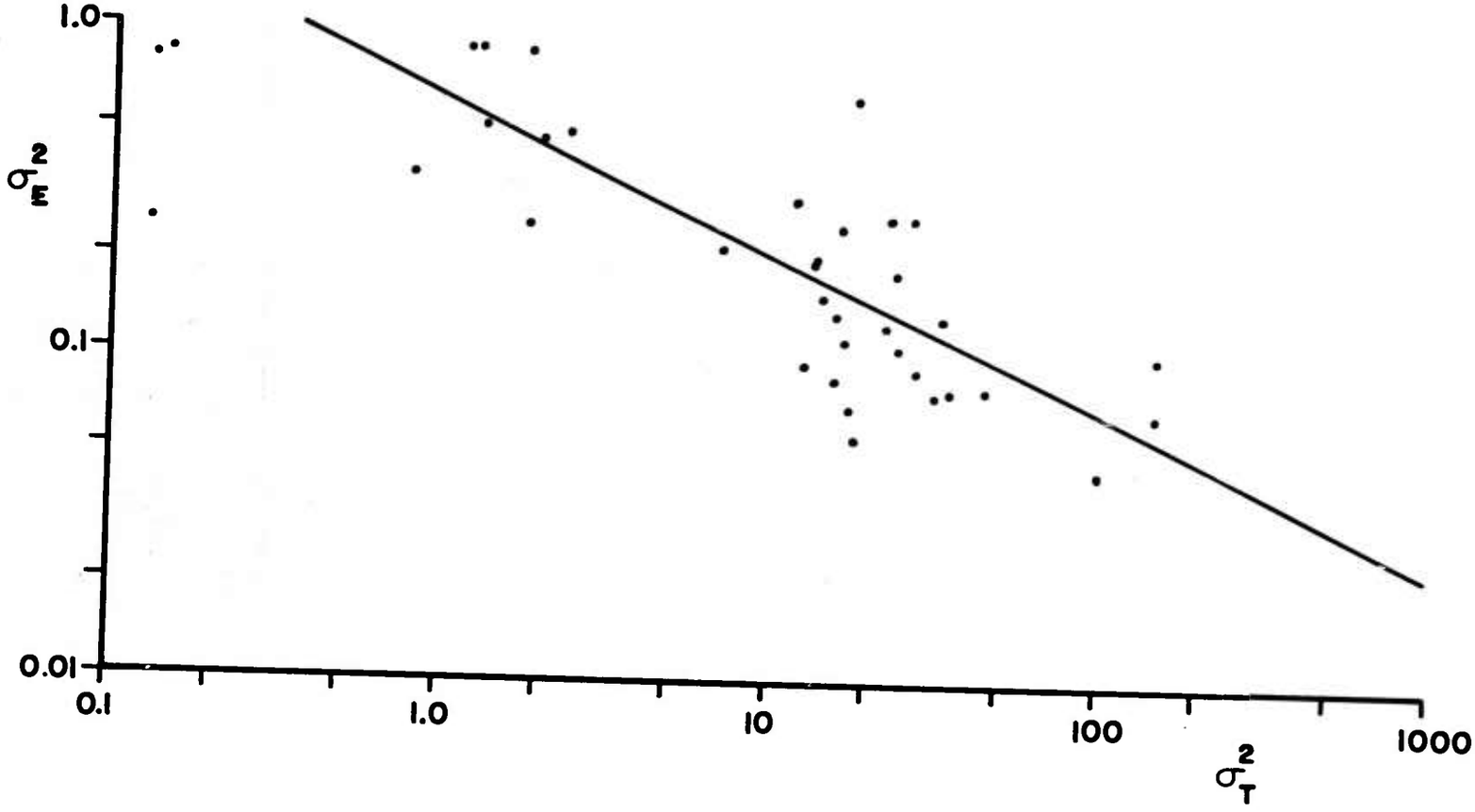

Figure 6

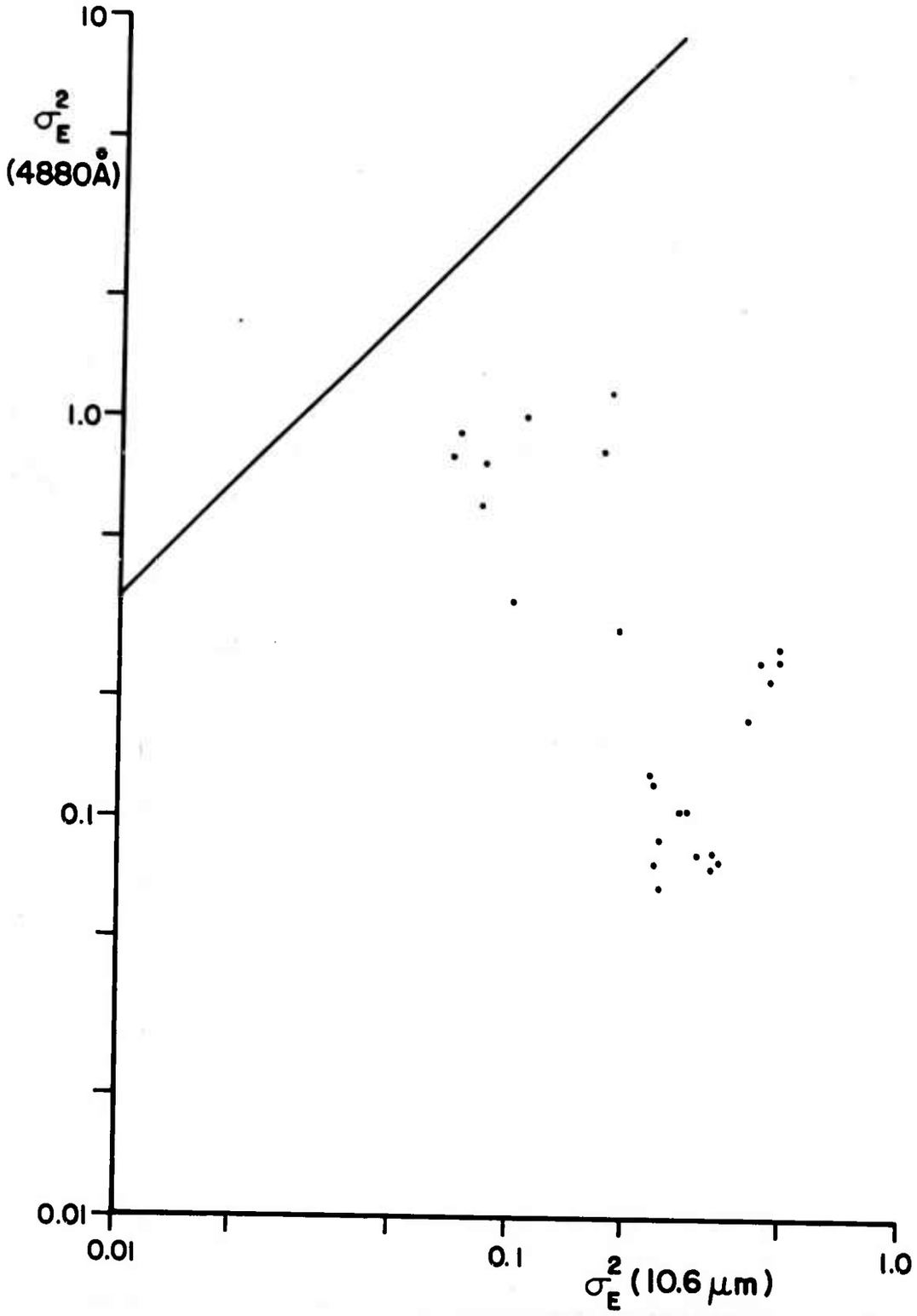

Figure 7

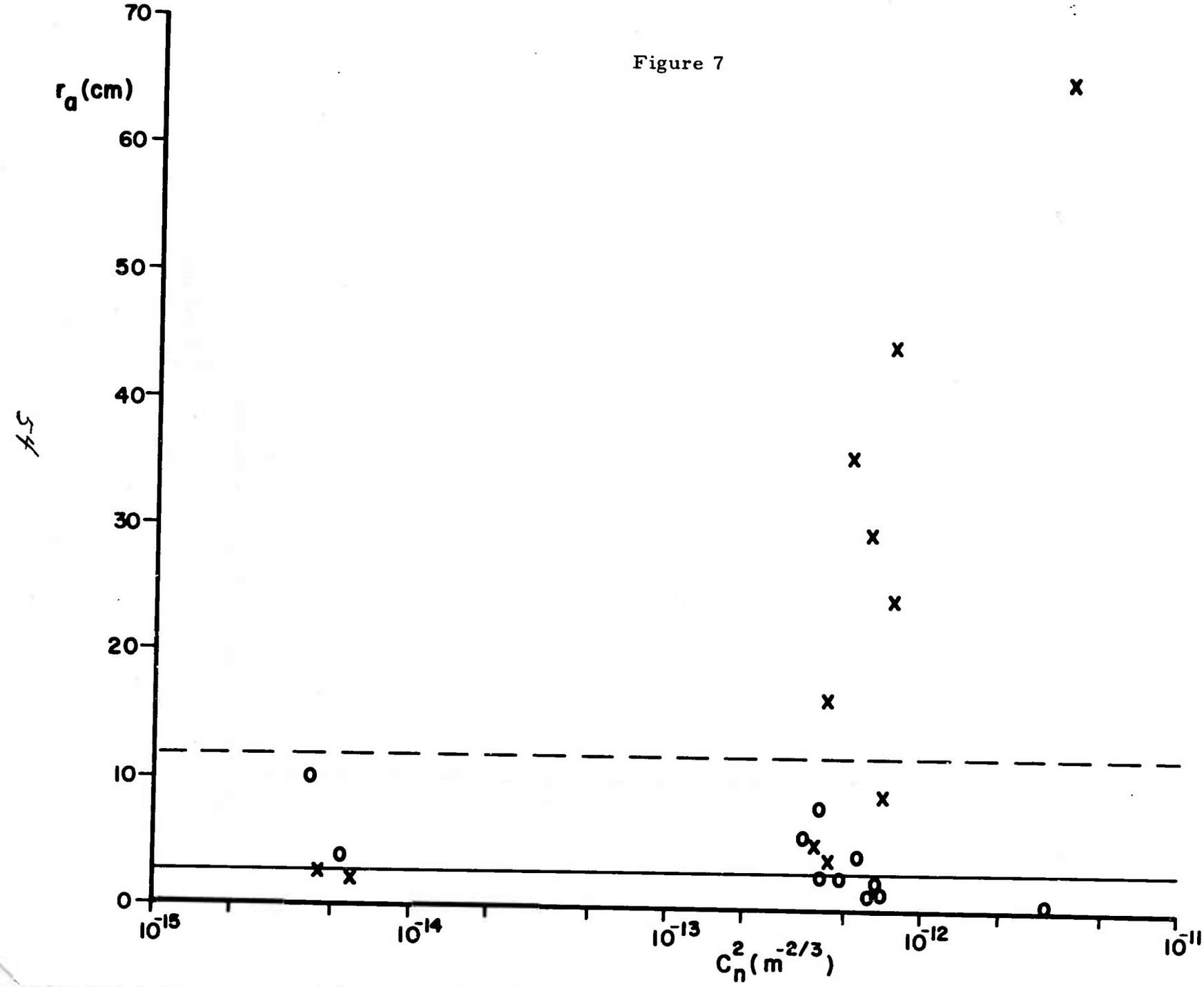

Figure 8

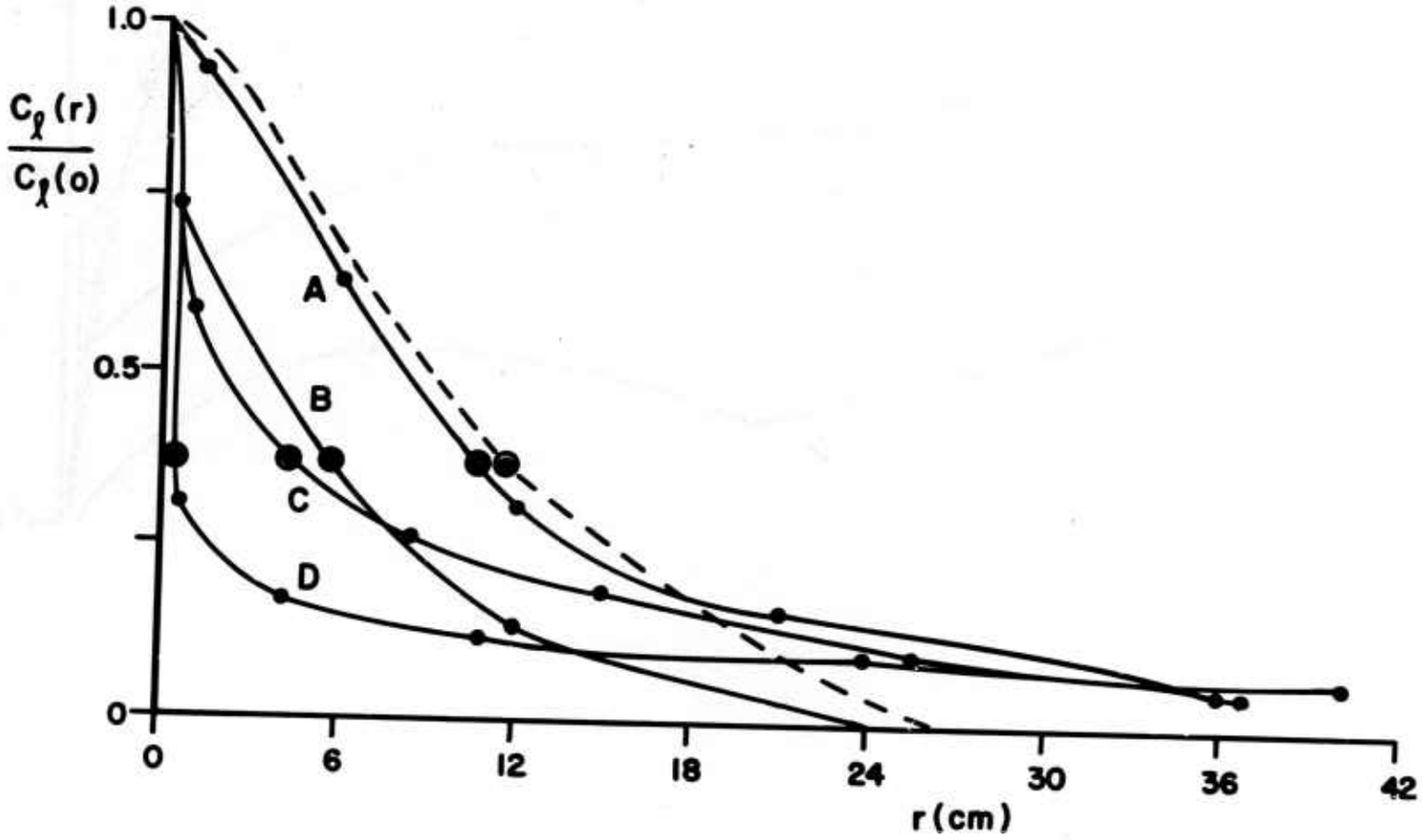

Figure 9

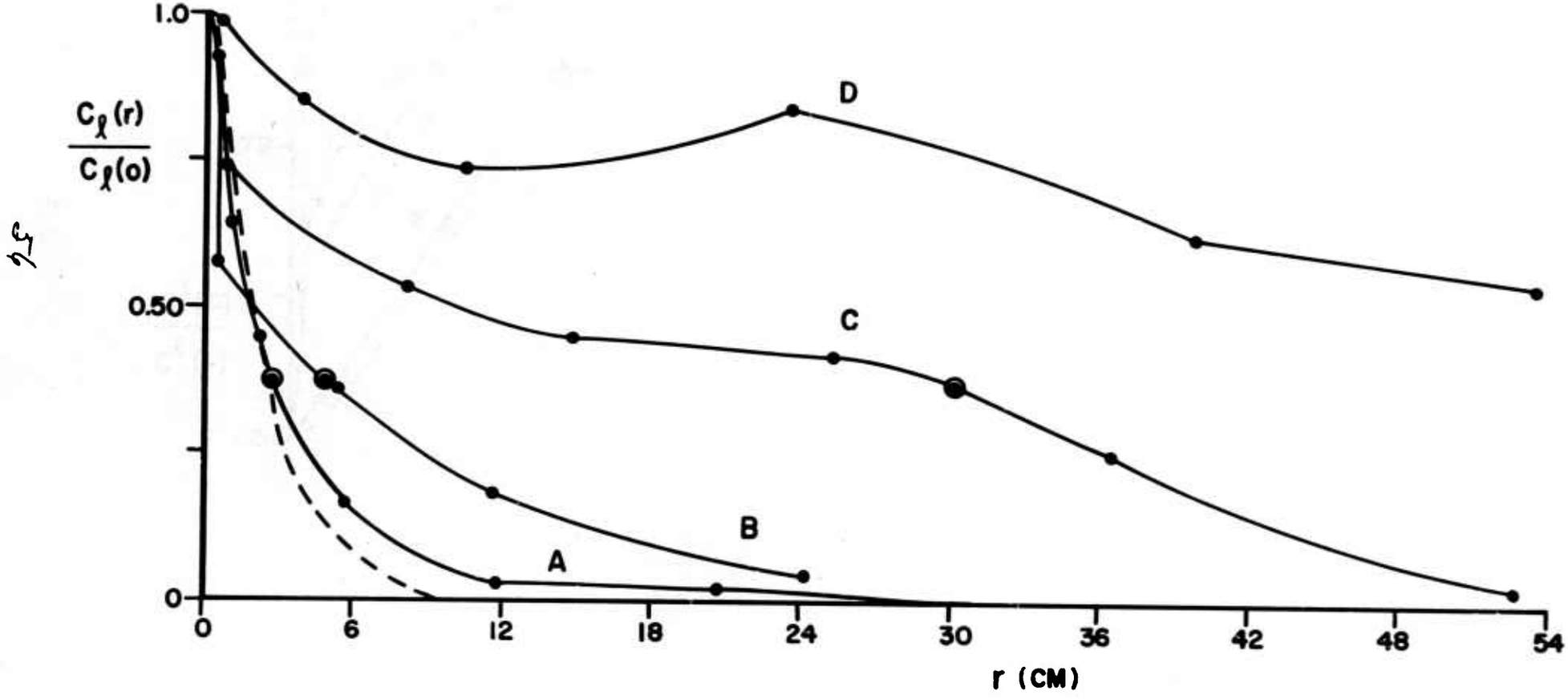

Figure 10

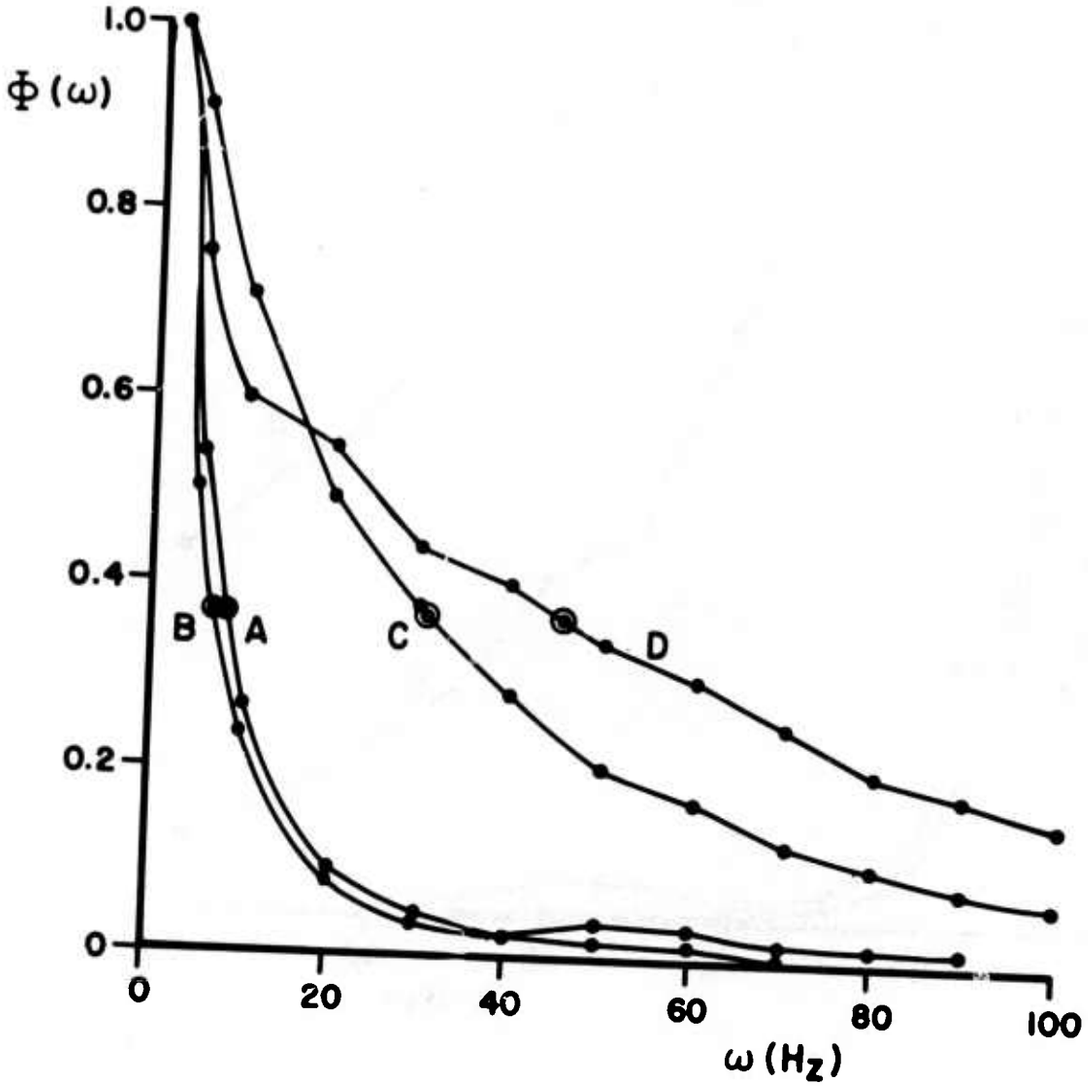

Figure 11

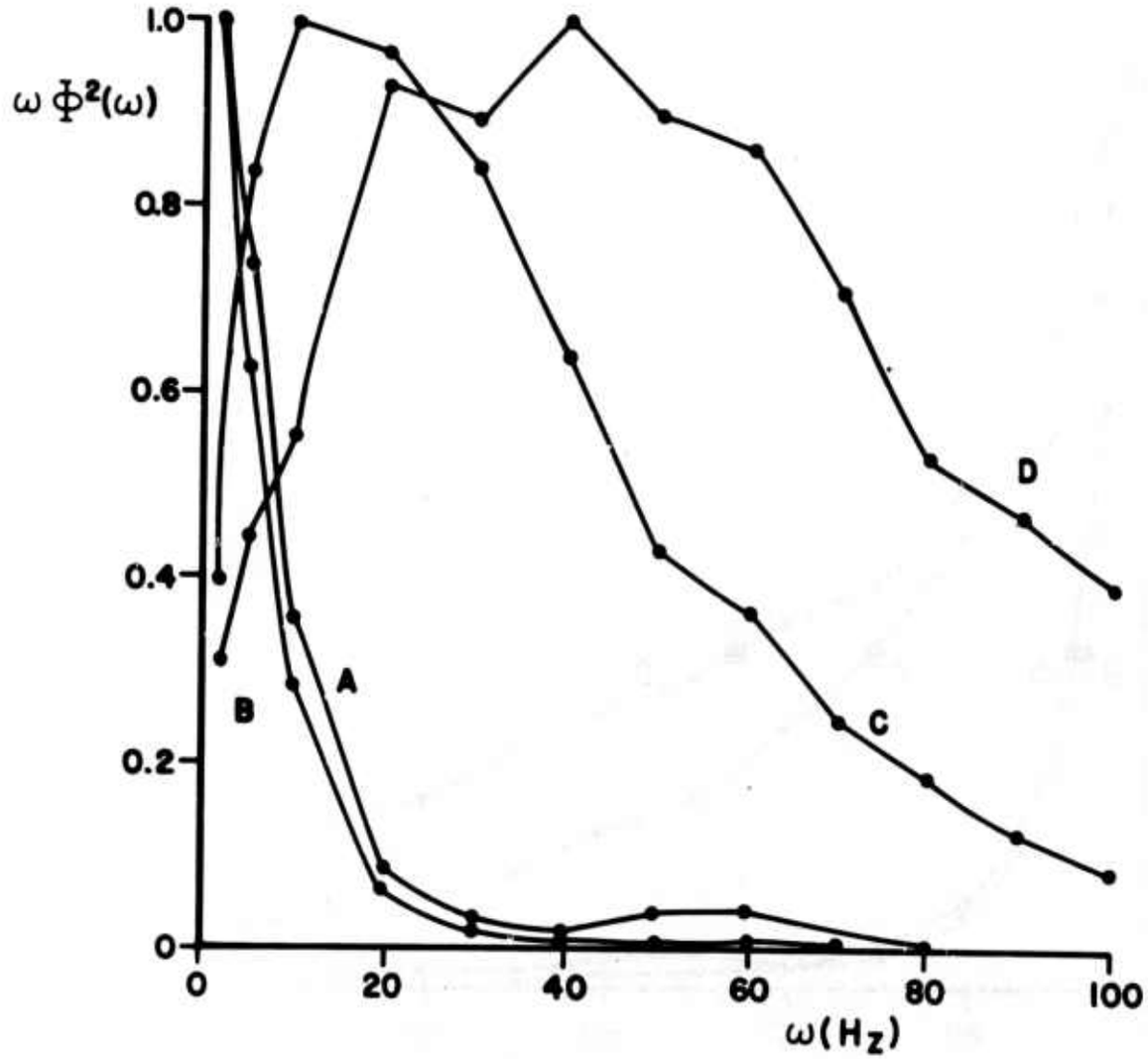

Figure 12

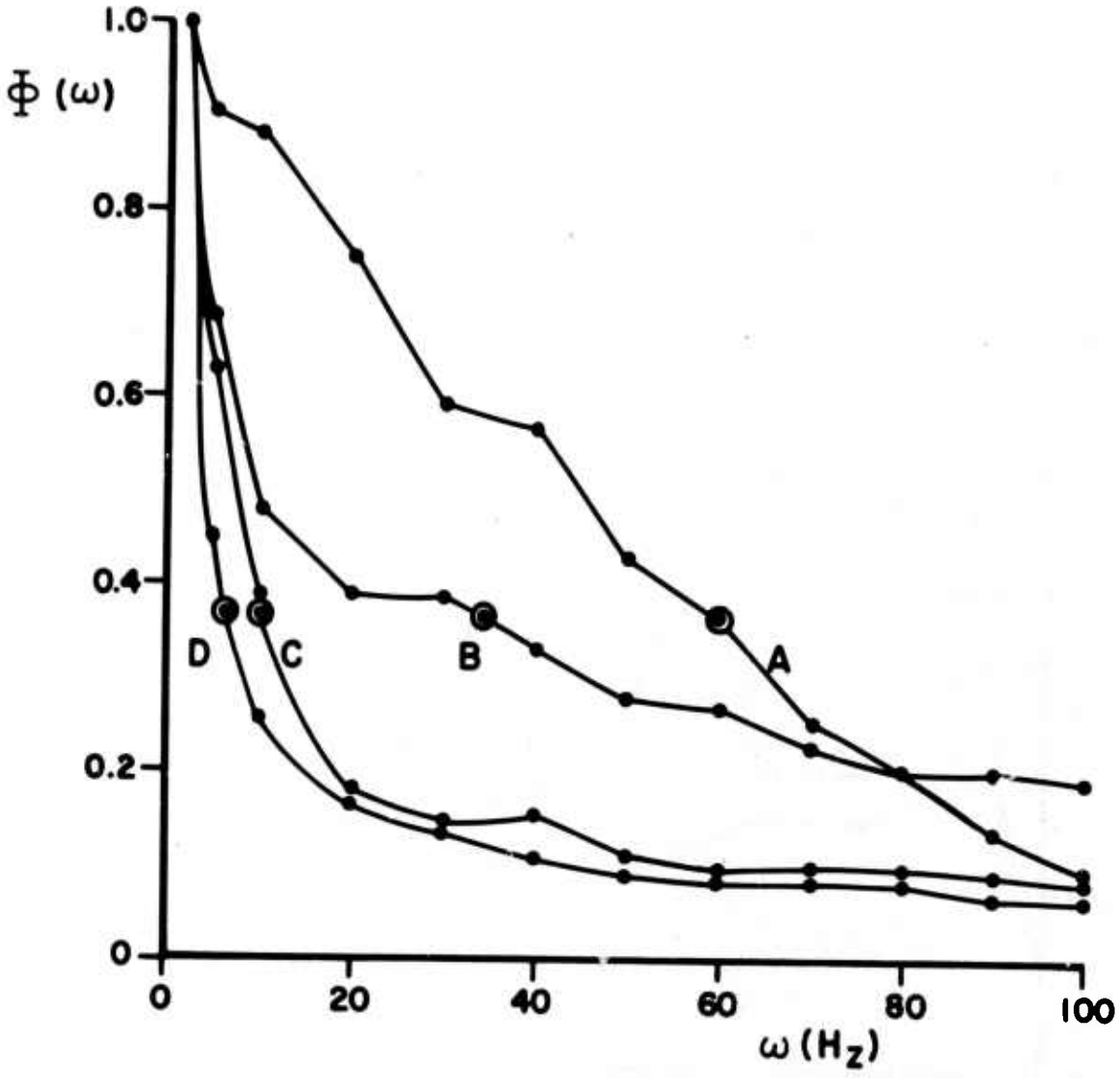

Figure 13

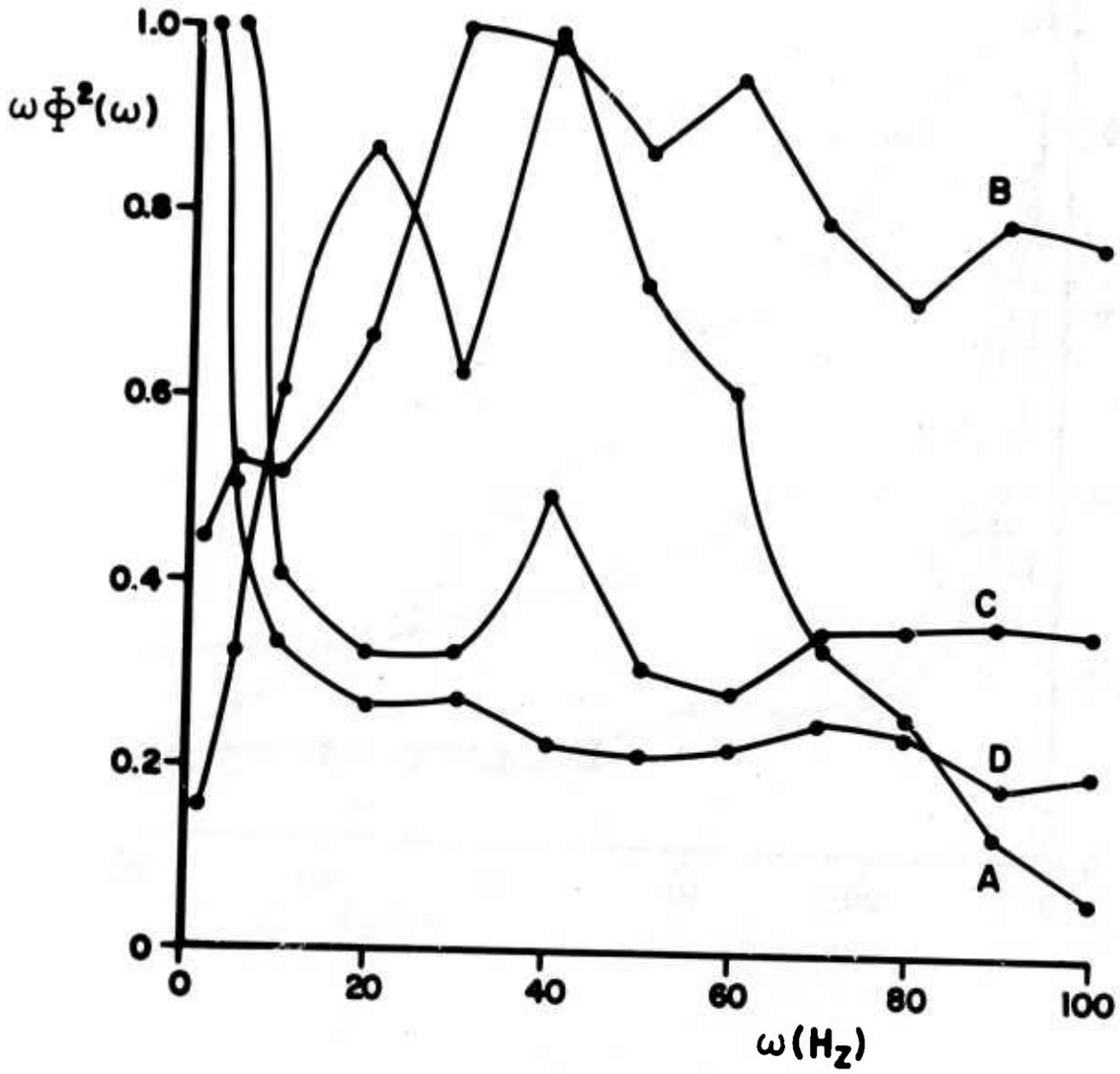

Figure 14

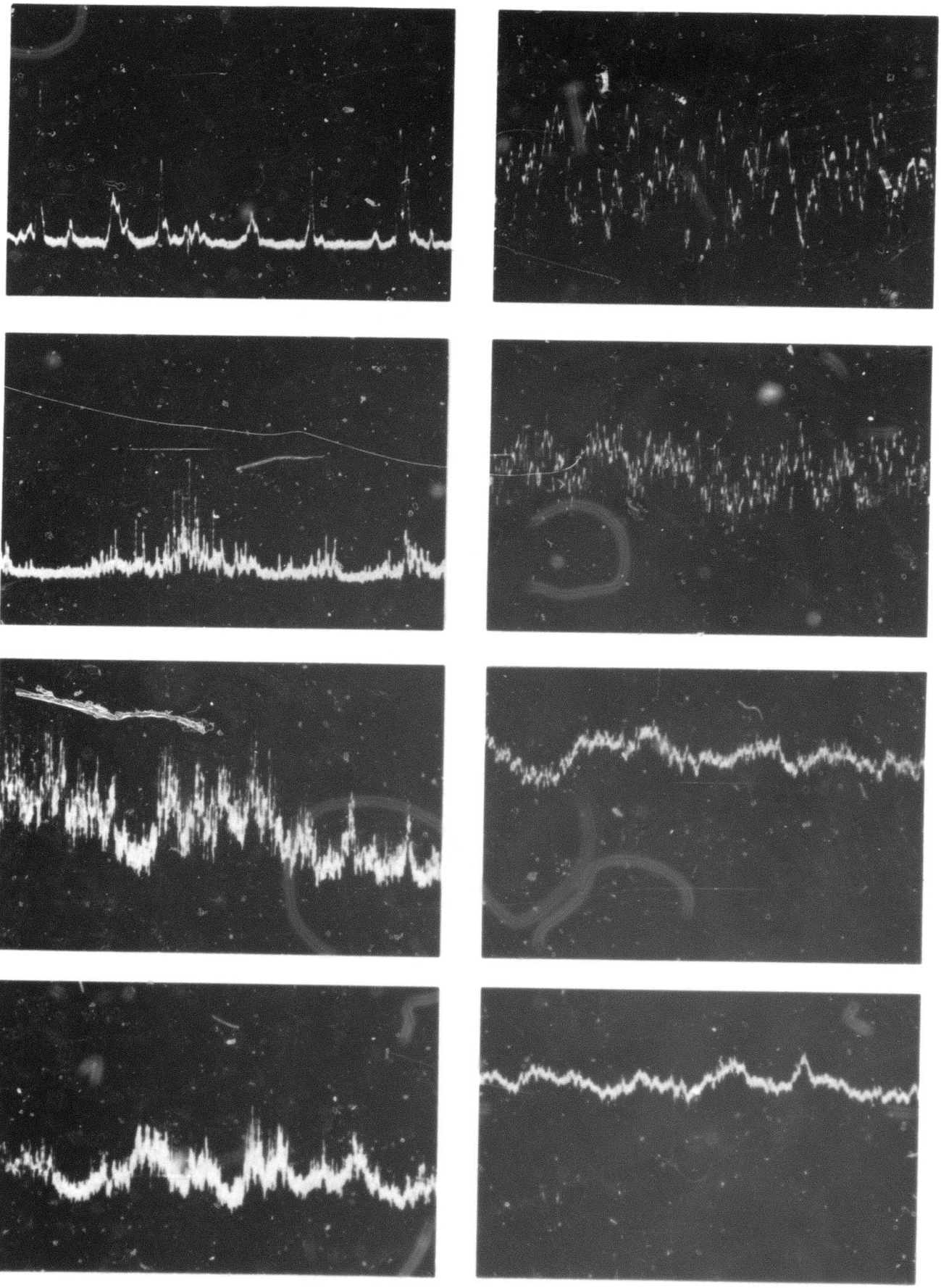

Figure 15

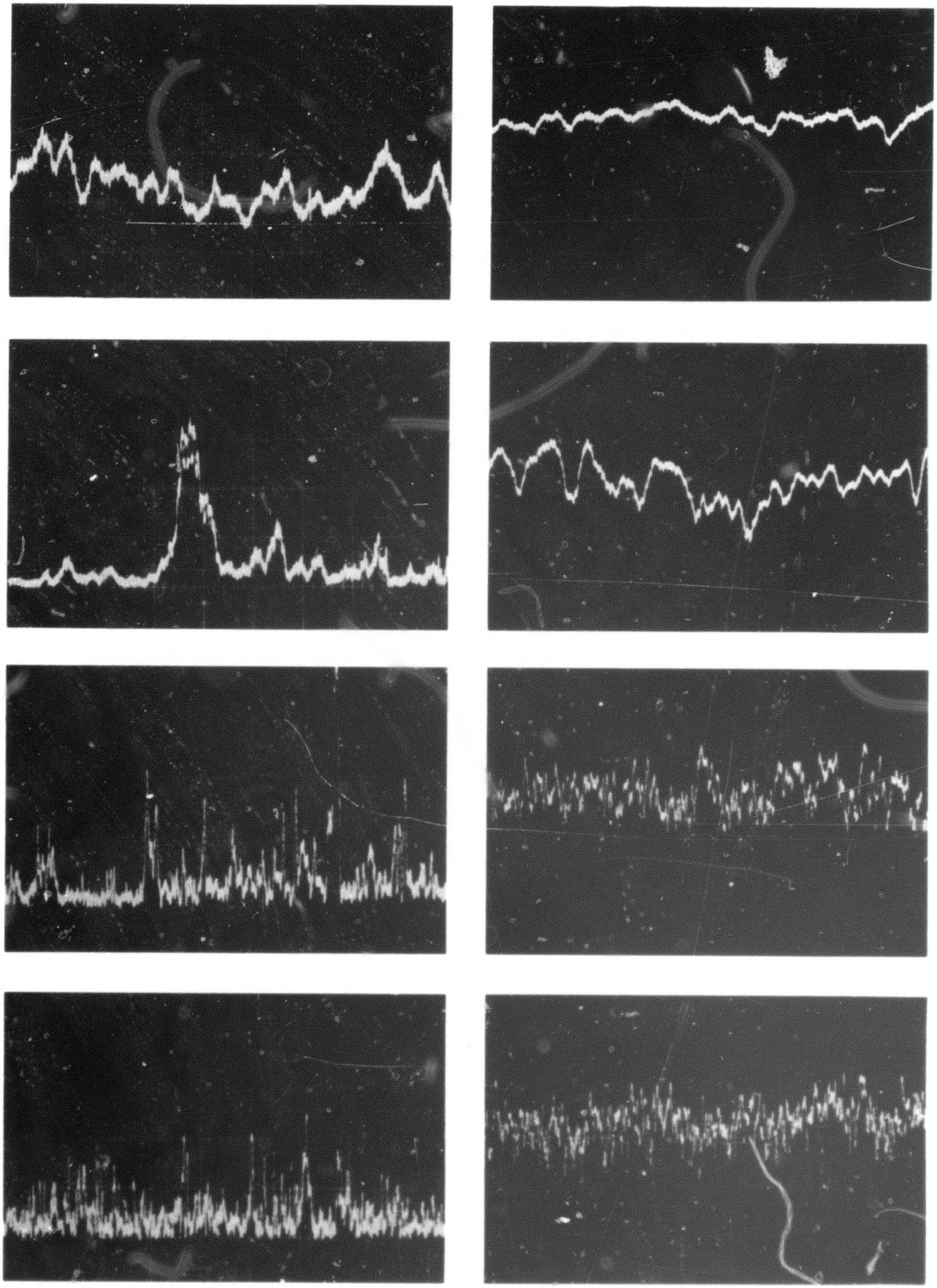

Figure 16

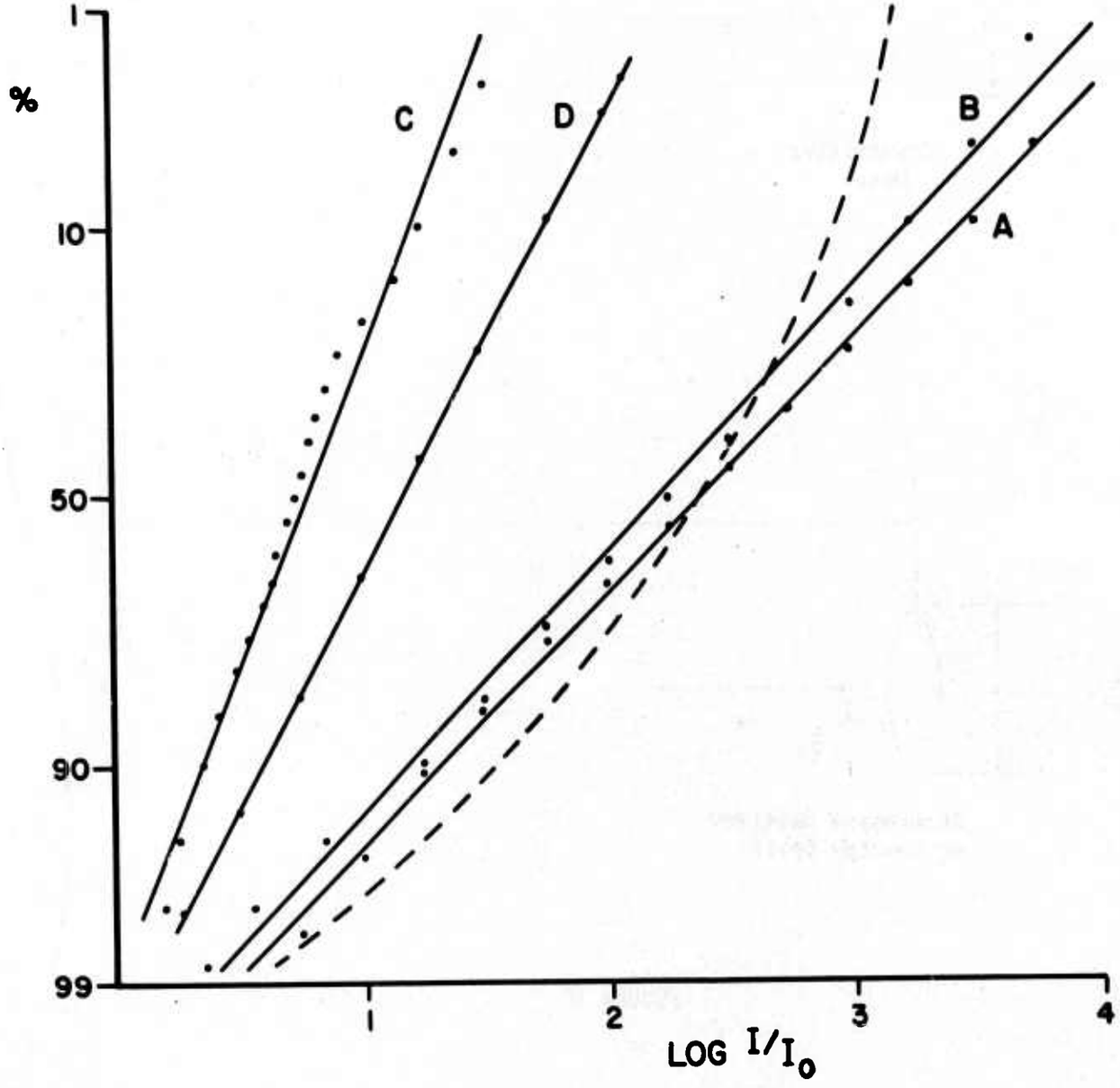

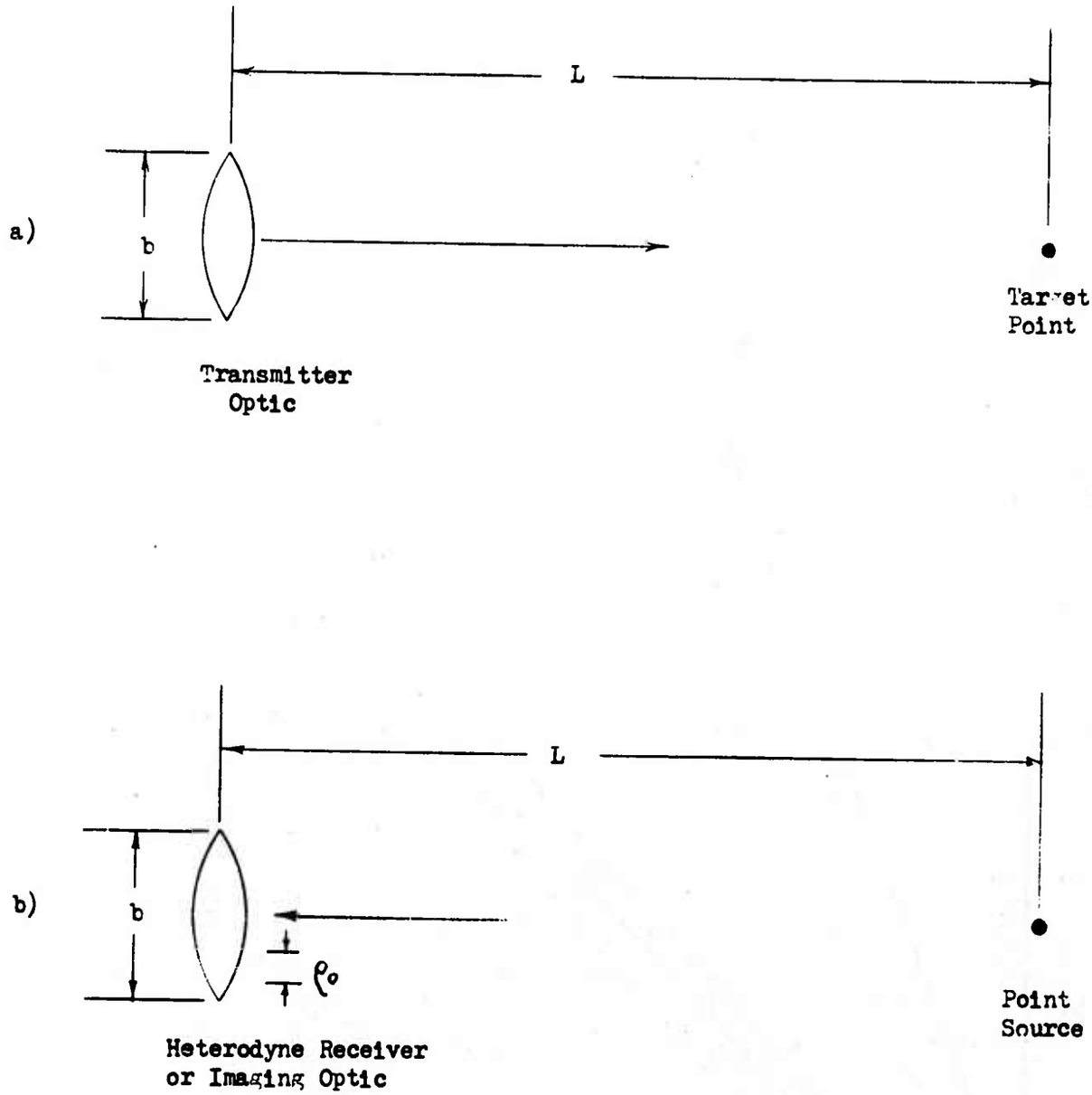
a)
L
b
Target
Point
Transmitter
Optic
b)
L
b
ρ_o
Point
Source
Heterodyne Receiver
or Imaging Optic

FIGURE 17

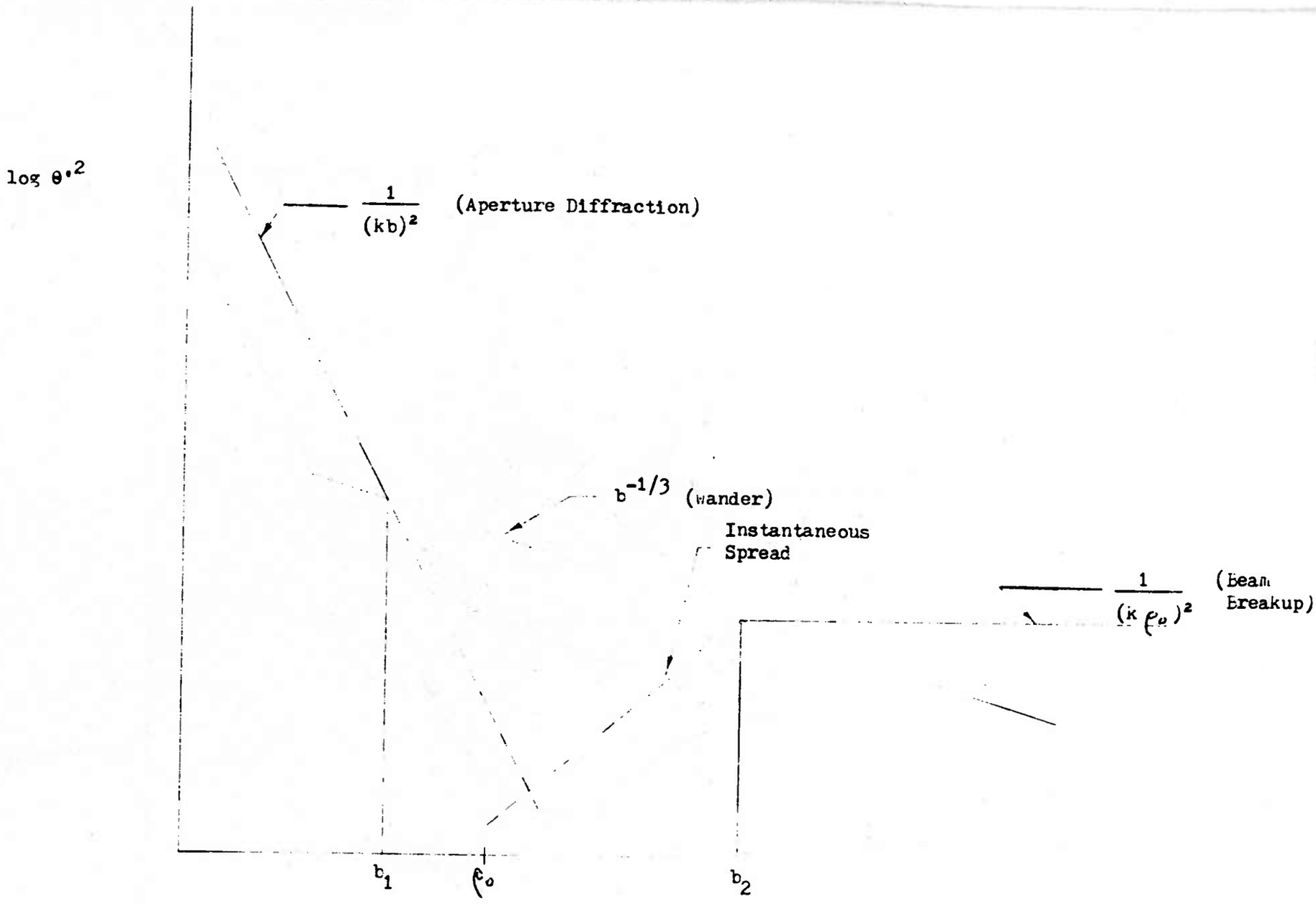
log θ'²
1/(kb)² (Aperture Diffraction)
b^-1/3 (Wander)
Instantaneous Spread
1/(k ρ₀)² (Beam Breakup)
b₁
ρ₀
b₂
log b

FIGURE 18

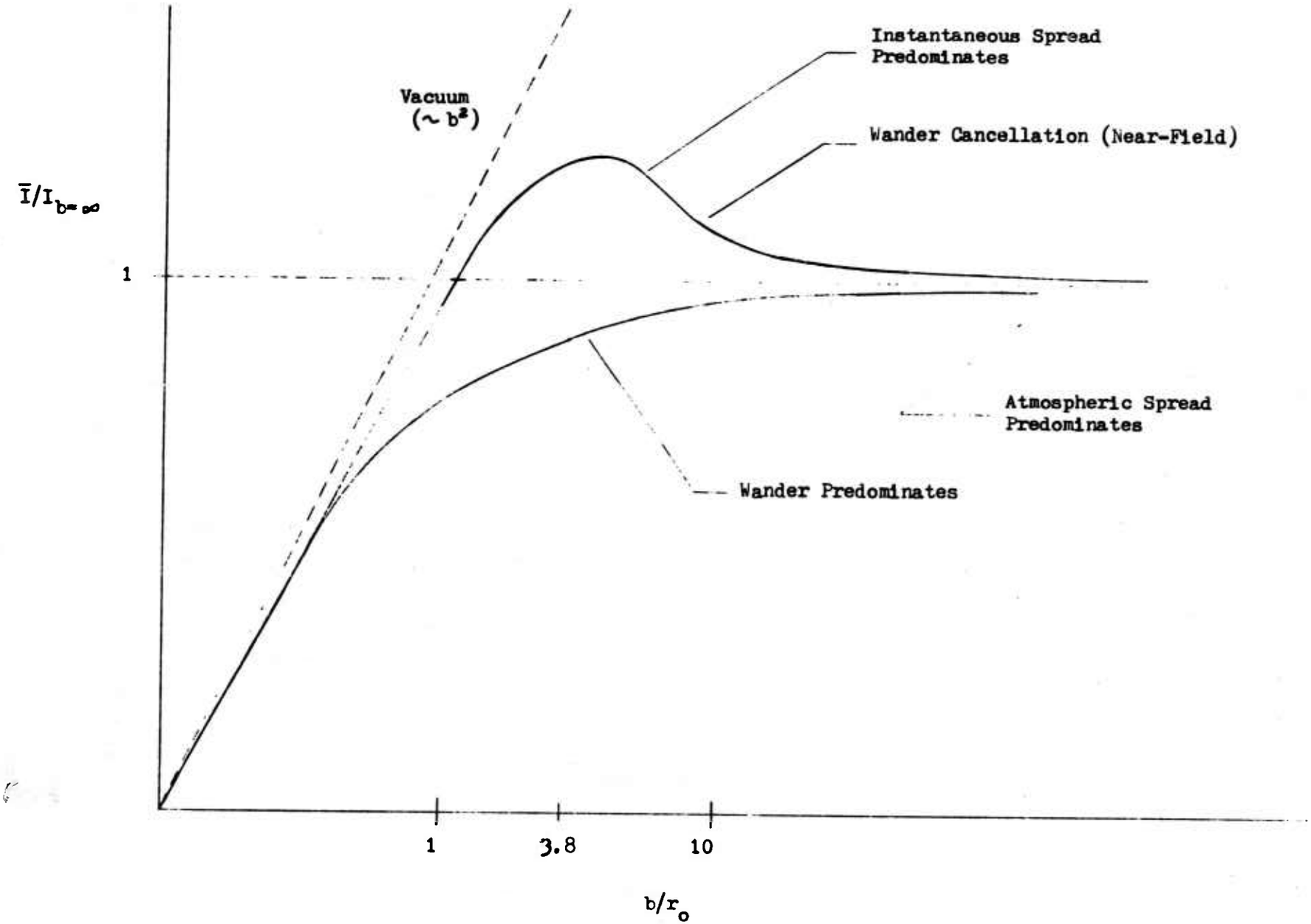
Instantaneous Spread
Predominates
Vacuum
(~ b²)
Wander Cancellation (Near-Field)
$\bar{I}/I_{b=\infty}$
1
Atmospheric Spread
Predominates
Wander Predominates
1
3.8
10
b/r_o

FIGURE 19

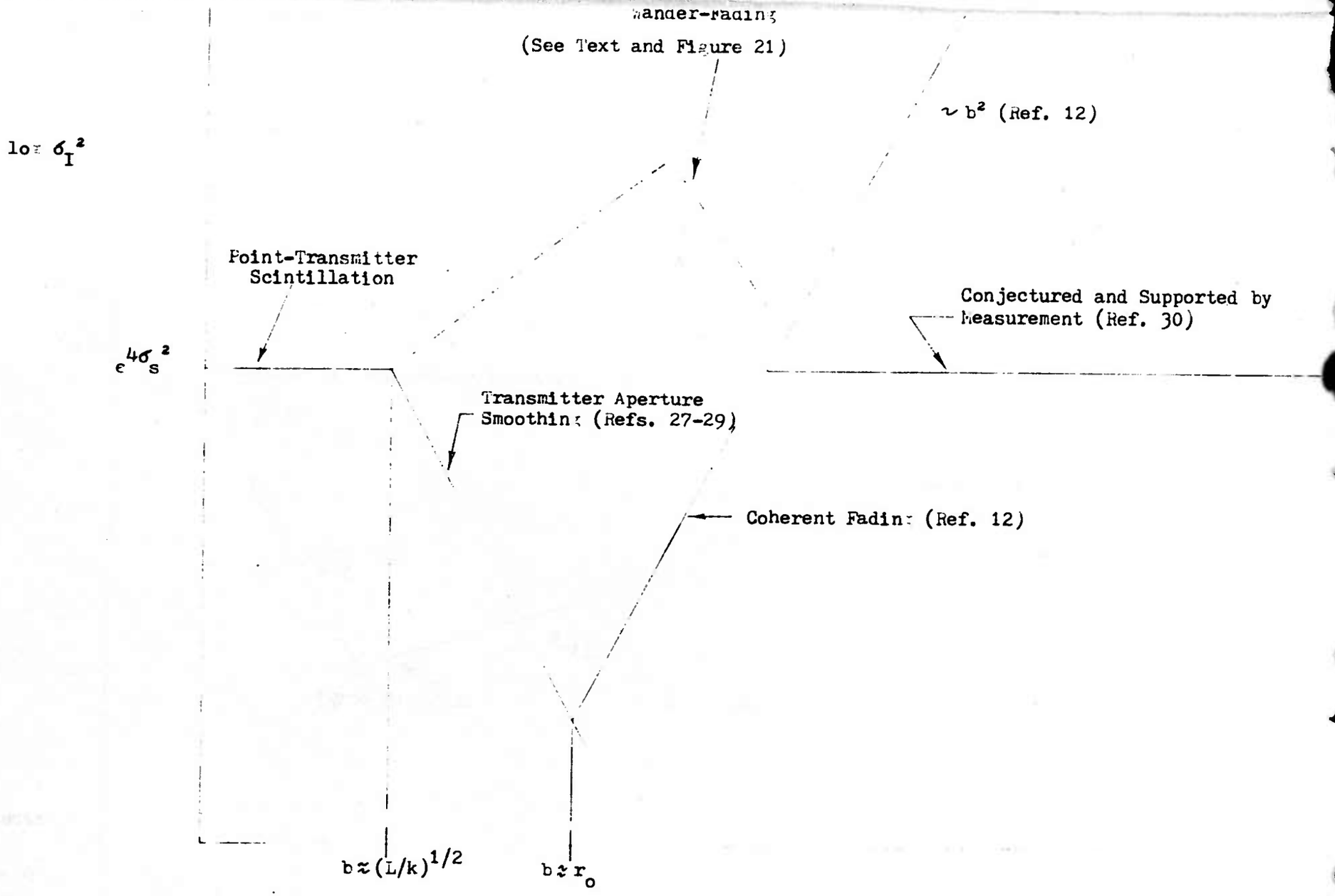
Wander-Fading
(See Text and Figure 21)
$\sim b^2$ (Ref. 12)
log σ_I^2
Point-Transmitter Scintillation
Conjectured and Supported by Measurement (Ref. 30)
$e^{4\sigma_s^2}$
Transmitter Aperture Smoothing (Refs. 27-29)
Coherent Fading (Ref. 12)
$b \approx (L/k)^{1/2}$
$b \approx r_o$
log b

FIGURE 20

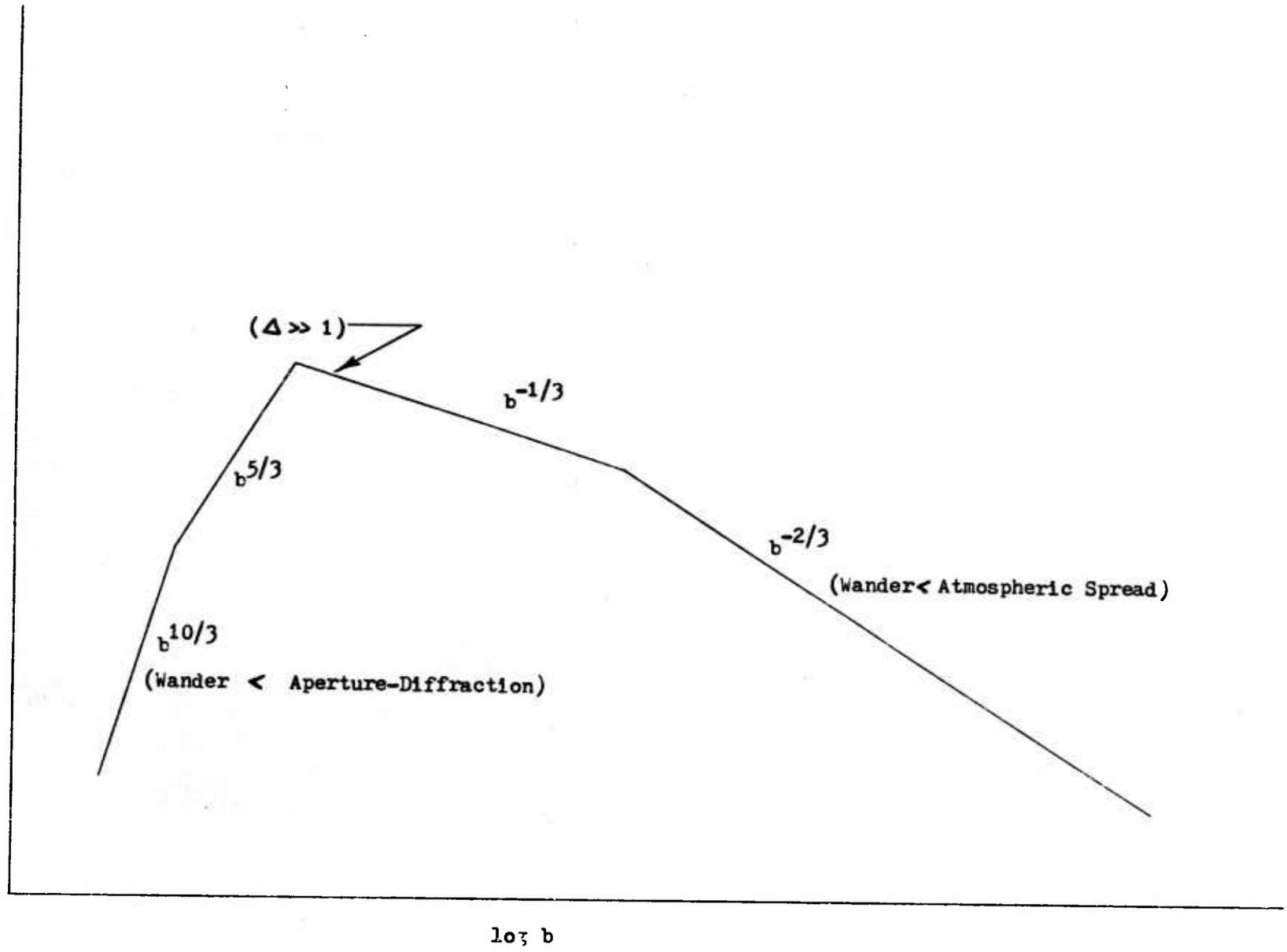
log σ_I^2
(Wander)
($\Delta \gg 1$)
$b^{-1/3}$
$b^{5/3}$
$b^{-2/3}$
(Wander< Atmospheric Spread)
$b^{10/3}$
(Wander < Aperture-Diffraction)
log b

FIGURE 21

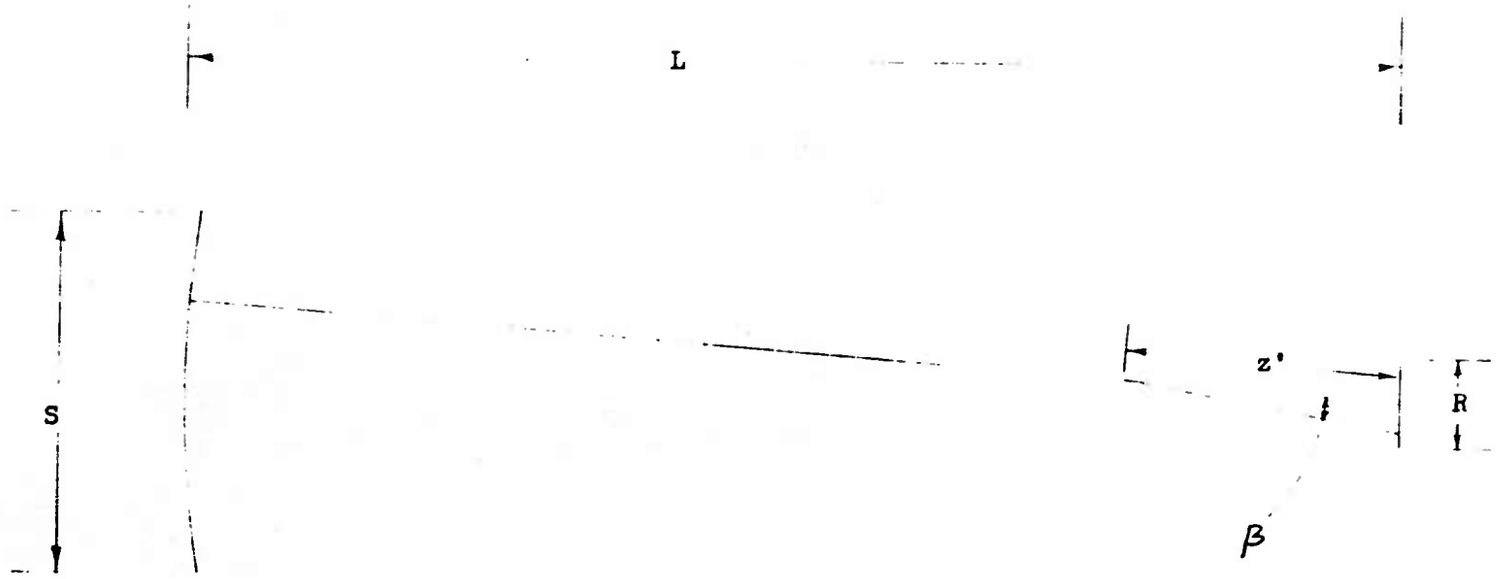

FIGURE 22

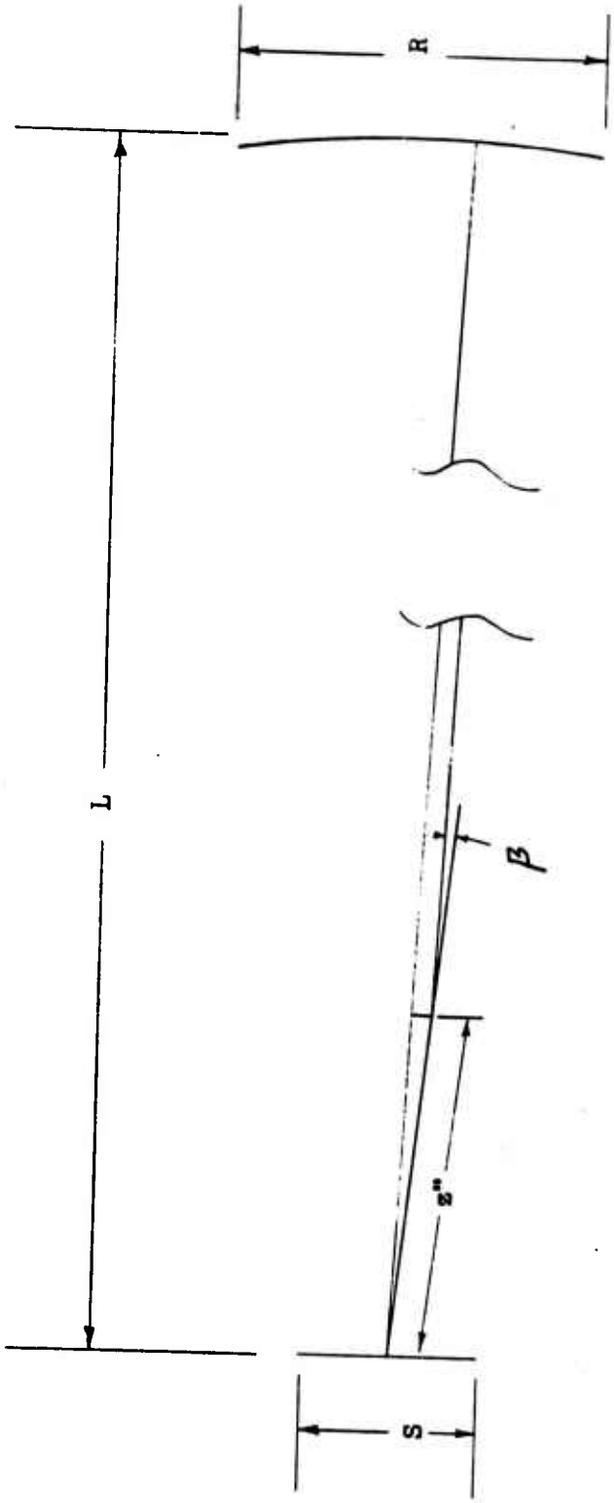

FIGURE 23

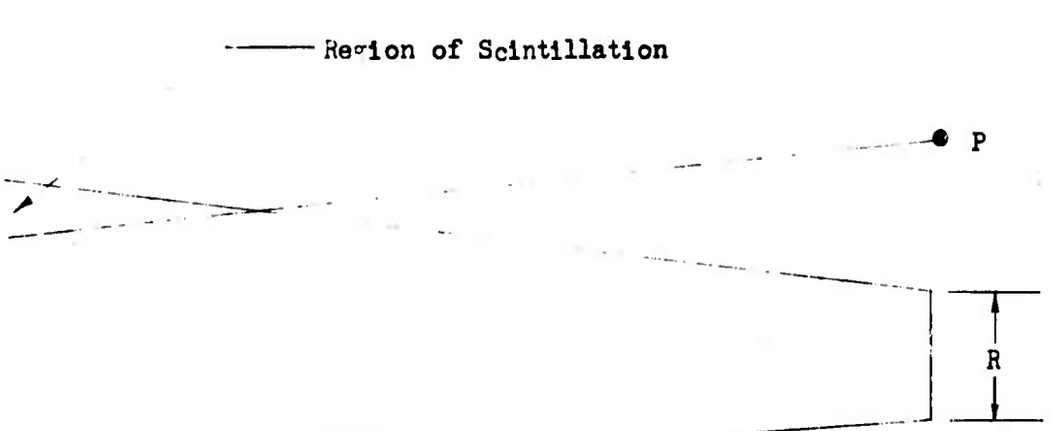

FIGURE 24

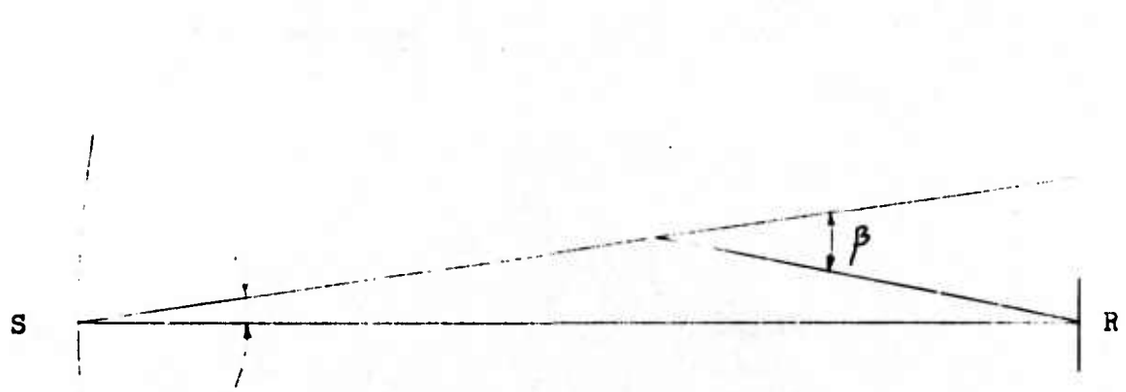

FIGURE 25

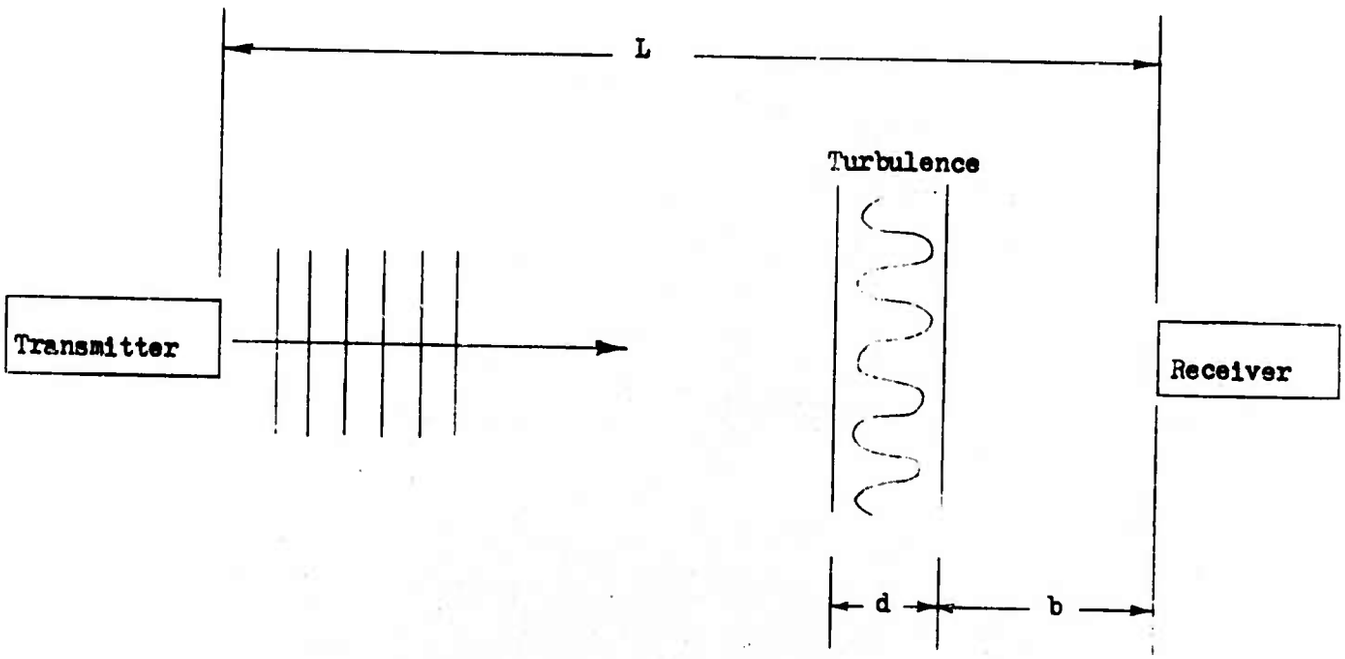

FIGURE 26

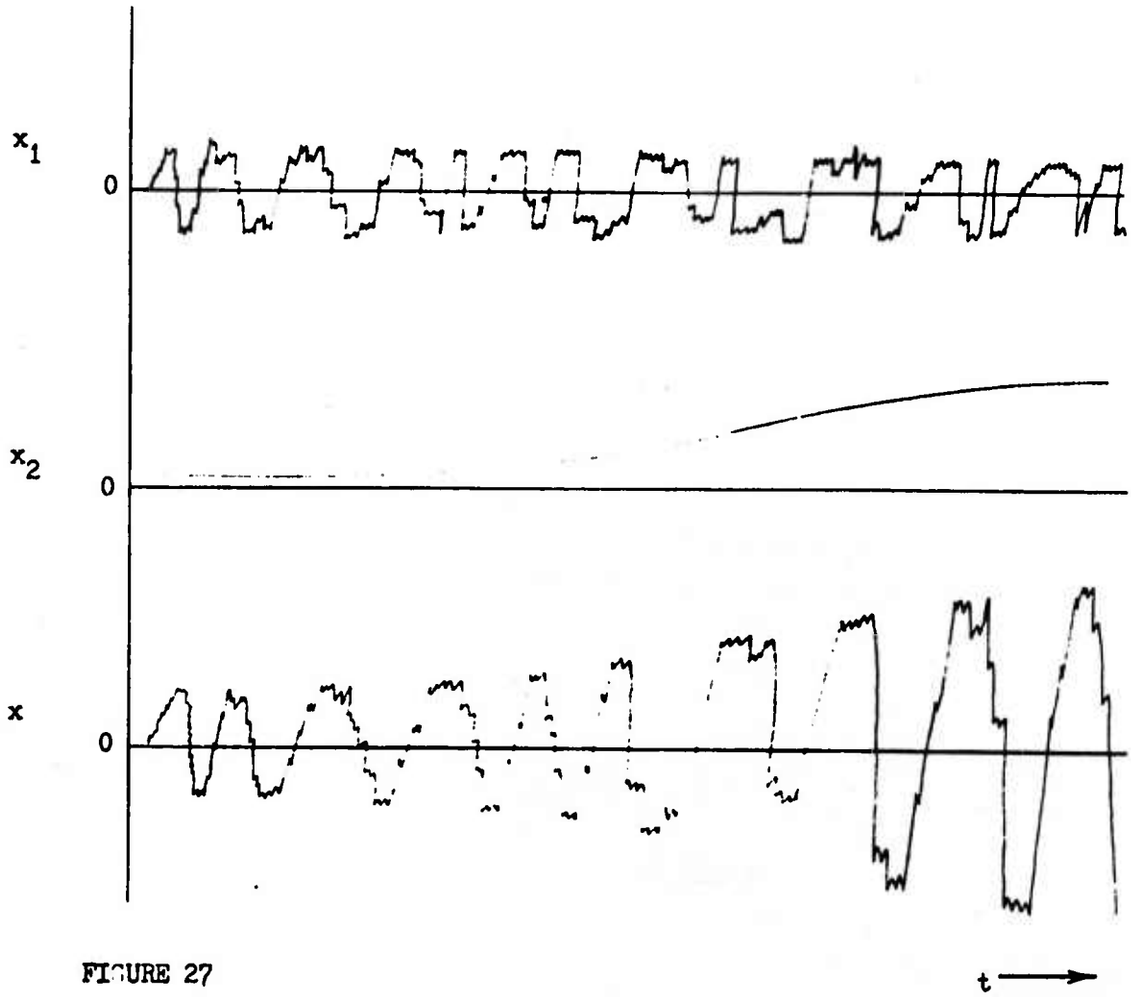

FIGURE 27

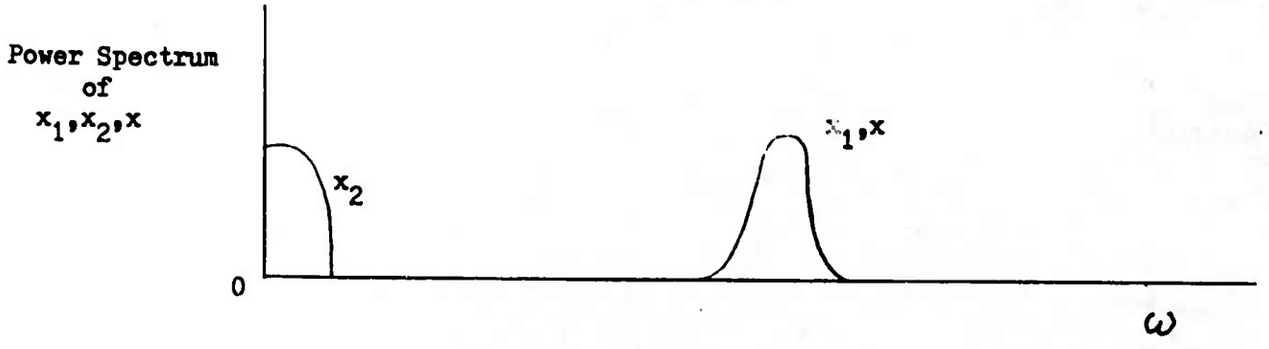

FIGURE 28

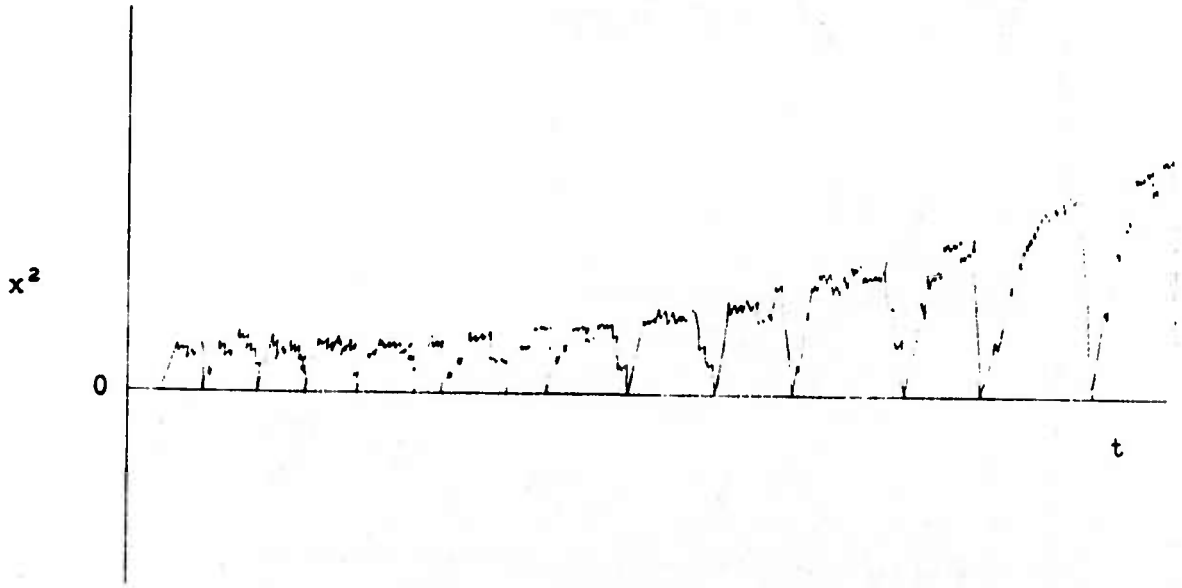

FIGURE 29

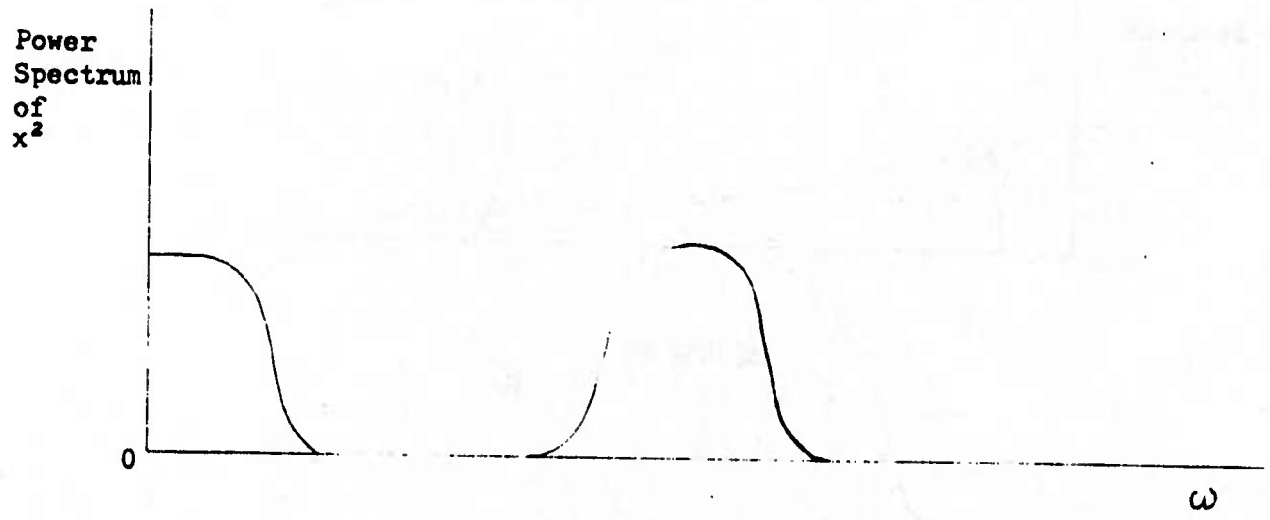

FIGURE 30